Cell Reports

Article

Sen1 and Rrm3 ensure permissive topological conditions for replication termination

Graphical abstract

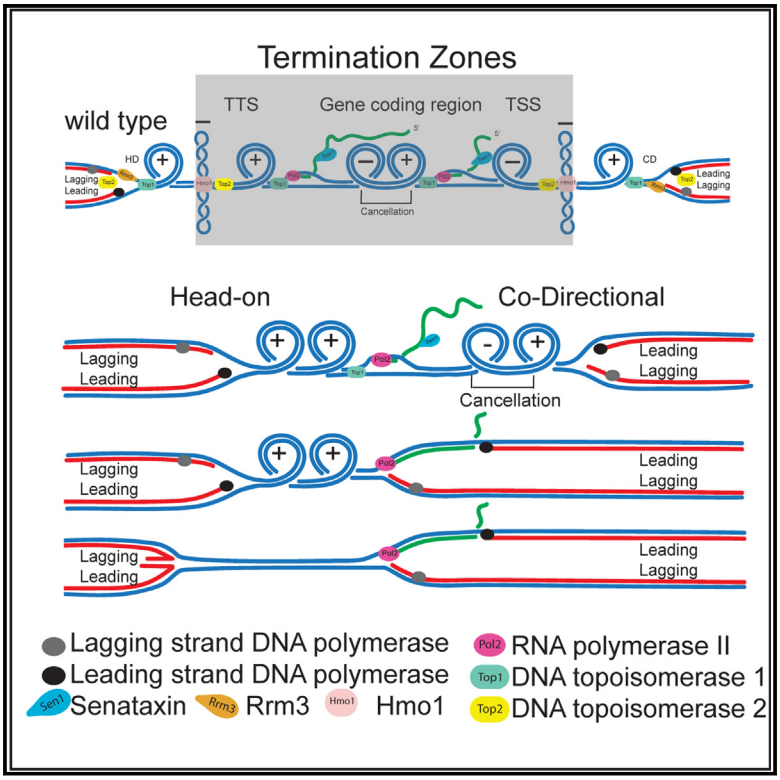

Highlights

- Rrm3 and Sen1 assist replication termination
- Rrm3 and Sen1 restrain Top1 and Top2 at *TER*s and telomeres
- Rrm3 and Sen1 helicases prevent aberrant topological events at *TER*s
- Positive supercoiling accumulation induces fork reversal at *TER*s

Authors

Ramveer Choudhary, Joanna Niska-Blakie, Mohamood Adhil, Giordano Liberi, Yathish Jagadheesh Achar, Michele Giannattasio, Marco Foiani

Correspondence

marco.foiani@ifom.eu

In brief

Replicon fusion is topologically challenging. Replication termination occurs at *TER* zones and telomeres. Choudhary et al. show that replication termination is assisted by transcription and by Sen1 and Rrm3 helicases that coordinate the activities of Top1 and Top2 topoisomerases at TERs and telomeres.

Choudhary et al., 2023, Cell Reports *42*, 112747
July 25, 2023
https://doi.org/10.1016/j.celrep.2023.112747

CellPress

Cell Reports

CellPress
OPEN ACCESS

Article

Sen1 and Rrm3 ensure permissive topological conditions for replication termination

Ramveer Choudhary,[1] Joanna Niska-Blakie,[1] Mohamood Adhil,[1,4] Giordano Liberi,[2] Yathish Jagadheesh Achar,[1,5] Michele Giannattasio,[1,3] and Marco Foiani[1,3,6,*]

[1]IFOM ETS - The AIRC Institute of Molecular Oncology, Via Adamello 16, 20139 Milan, Italy
[2]Istituto di Genetica Molecolare "Luigi Luca Cavalli-Sforza," CNR, Pavia, Italy
[3]Università degli Studi di Milano, Via Festa del Perdono, 7, 20122 Milan, Italy
[4]Present address: Enhanc3D Genomics Ltd, Cambridge, UK
[5]Present address: Centre for DNA Fingerprinting and Diagnostics (CDFD), Hyderabad, India
[6]Lead contact
*Correspondence: marco.foiani@ifom.eu
https://doi.org/10.1016/j.celrep.2023.112747

SUMMARY

Replication forks terminate at *TER*s and telomeres. Forks that converge or encounter transcription generate topological stress. Combining genetics, genomics, and transmission electron microscopy, we find that Rrm3^{hPif1} and Sen1^{hSenataxin} helicases assist termination at *TER*s; Sen1 specifically acts at telomeres. *rrm3* and *sen1* genetically interact and fail to terminate replication, exhibiting fragility at termination zones (*TER*s) and telomeres. *sen1rrm3* accumulates RNA-DNA hybrids and X-shaped gapped or reversed converging forks at *TER*s; *sen1*, but not *rrm3*, builds up RNA polymerase II (RNPII) at *TER*s and telomeres. Rrm3 and Sen1 restrain Top1 and Top2 activities, preventing toxic accumulation of positive supercoil at *TER*s and telomeres. We suggest that Rrm3 and Sen1 coordinate the activities of Top1 and Top2 when forks encounter transcription head on or codirectionally, respectively, thus preventing the slowing down of DNA and RNA polymerases. Hence Rrm3 and Sen1 are indispensable to generate permissive topological conditions for replication termination.

INTRODUCTION

DNA and RNA polymerases move on the same DNA template to replicate and transcribe chromosomes. In bacteria, which have a single replication origin, there is a bias toward codirection of replication and transcription,[1] and the two forks generated by the origin, while converging at the end of replication, experience a regulated termination process mediated by the *Tus*/*Ter* system.[2] In eukaryotes, replication initiates at multiple origins and, consequently, replication forks continuously experience head on (HD) and co-directional (CD) clashes with transcription. The collision between converging forks during replication termination occurs at termination zones (*TER*s) and is facilitated by transcription,[3] while those forks proximal to chromosome ends terminate at telomeres. Advancing DNA and RNA polymerases generate topological stress by imposing torsional stress on the DNA duplex and their progression depends on the action of DNA topoisomerases, specialized enzymes, which resolve the topological complexity created by the replication and transcription machineries.[4,5] Topoisomerases are particularly relevant when forks encounter transcription units or when they converge during replication termination.[3,4,6]

In *Saccharomyces cerevisiae*, two topoisomerases, Top1 and Top2, assist replication and transcription.[4] Advancing replisomes rotate, generating positive supercoil in front of the fork and precatenanes behind the forks.[4] Most likely, Top1 resolves positive supercoil in front of the fork, while Top2 resolves precatenation behind the fork.[4,7] Advancing RNA polymerases generate positive supercoil in the front and negative supercoil in the back.[8] Top1 and Top2 can resolve both negative and positive supercoil generated during transcription.[9] The architecture of transcribed genes is mediated by under-wound DNA at gene boundaries and over-wound DNA within coding regions.[10] Top2 and Hmo1 (an HMGB-like protein) preserve negative supercoil at gene boundaries, while Top1 acts at coding regions.[10] The collision between converging forks also generates topological stress[4] and replication termination at *TER*s is mediated by Top2.[3,11] While in yeast the topological context of telomere-mediated fork termination is unclear, in mammals it has been proposed that transcription drives T-loop formation and that Topoisomerase II alpha assists replication of telomeres.[12–14]

Replication termination represents one of the most challenging events from the topological point of view. Accordingly, some *TER*s have been identified as fragile sites.[15]

Replication-induced topological stress has relevant implications for the mechanical properties of the chromosomes; eukaryotic chromosomes are in physical contact with the nuclear envelope and the nucleolus and are governed by internal mechanical forces, implying that information can travel by direct mechanical linkage from the chromosomes outward and from external

components inward to the chromosomes.[16] When a replication fork encounters a transcription unit, the local topological stress[4] generates mechanical forces that can rapidly spread through chromatin domains, eventually reaching chromatin-associated structures such as the nucleolus and the nuclear envelope.[17,18] These mechanical signals activate a specialized mechano-transduction pathway that uncouples mRNA transcription from export through the nuclear envelope, thus facilitating fork advance.[17]

Replication fork advance is assisted by specialized DNA helicases. Rrm3 is a replisome associated protein that travels with a 5′ to 3′ polarity, mediating fork advance through natural pausing sites such as telomers, tRNAs, and TERs.[3,19–28] *S. cerevisiae* Sen1 (Senataxin in humans) helicase belongs to the superfamily I RNA/DNA helicases and counteracts RNA/DNA hybrids formation during transcription by interacting directly with RNA polymerase II (RNPII).[29–33] Sen1 has also been involved in facilitating fork advance at transcribed regions.[34,35]

We found that Rrm3 and Sen1 helicases assist replicon fusion at *TER*s, while Sen1 specifically mediates replication termination at telomeres. Double mutants exhibit a synthetic interaction, fail to complete replication, exhibit lagging chromosomes, and experience fragility at *TER*s and telomeres. *sen1*, but not *rrm3*, accumulates RNPII at *TER*s and telomeres. We show that specifically *sen1 rrm3* cells exhibit aberrant converging forks in an X-gapped or reversed-fork conformation. We also found that Rrm3 and Sen1 restrain topoisomerase activities, preventing the accumulation of toxic positive supercoiling at *TER*s and telomeres. Altogether, our data suggest that Rrm3 and Sen1 generate permissive topological conditions for terminating replication at *TER*s and telomeres.

RESULTS

sen1 and *rrm3* exhibit a synthetic interaction and double mutants arrest in G2/M with lagging chromosomes

rrm3Δ mutants accumulate cruciform replication intermediates at a subset of *TER*s, characterized by the presence of RNPII-transcribed genes.[3] However, *rrm3Δ* mutants are viable and can still complete replication termination.[3,19,36–39] We reasoned that other helicase(s) might assist replication termination in the absence of Rrm3. We focused our attention on $Sen1^{Senataxin}$, a helicase involved in assisting replication fork progression at RNPII-transcribed genes.[32,34,40] Moreover, we identified *rrm3Δ* in a genetic screen aimed at identifying synthetic mutations with *sen1-1*. Genome-wide analysis[34] showed that Sen1 is enriched at RNPII-transcribed genes. We performed a meta-analysis of Sen1 high occupancy sites in G1, G2/M, and HU-arrested cells: while in G1 and G2/M Sen1 distribution paralleled the one of RNPII along the coding regions,[10] specifically in S-phase cells, Sen1 accumulated also at gene boundaries (Figures S1A and S1B). This particular S-phase Sen1 distribution may reflect the accumulation of the sub-population of Sen1 traveling with converging forks. Out of 71 *TER*s, 43 exhibited Sen1 accumulation in S-phase cells (p = 4.42E−06) (Table S1 and Figure S1B). Out of these 43 *TER*s, 35 contain RNPII-transcribed genes (Table S1). Five *TER*s (303, 603, 702, 1101, 1602) are characterized by transcription events, and three (704, 1504, 1604) by the presence of centromeres. We then addressed whether Sen1 plays any functional role at these *TER*s by using a conditional lethal $sen1^{degron}$ mutant.[34] Briefly, in the $sen1^{degron}$ genetic background (GAL-URL-HA-SEN1p), 2% galactose allows the expression of Sen1p, while 2% glucose causes Sen1p depletion (Figure S1C). Previous observations showed that, while wild-type (WT) cells accumulate hybrids along the coding regions, $sen1^{degron}$ mutants exhibit an aberrant and polar accumulation of hybrids also at transcription termination sites (TTSs).[10] $sen1^{degron}$ cells were released from G1 into S phase under limiting conditions (glucose) to monitor the genome-wide accumulation of RNA-DNA hybrids. $sen1^{degron}$ mutants exhibited a significantly higher accumulation of hybrids compared to WT cells in 33 *TER*s; of these, 26 contained RNPII-transcribed genes (p = 0.000161) (Table S1 and Figure S1D). We then focused our study on the genetic interaction between *sen1* and *rrm3*. Two parental haploid strains, carrying the *sen1-1* (*sen1-G1747D*) and *rrm3Δ* mutations, were crossed and then the diploid strain was subjected to sporulation and tetrad dissection. Spores were kept at the semi-permissive temperature for the *sen1-1* mutation. The double-mutant combinations exhibited a synthetic phenotype (Figure 1A). We then combined the *RRM3* deletion with the $sen1^{degron}$ mutation. In 0.05% galactose, the $sen1^{degron}$ mutant was slow growing, while the double-mutant $sen1^{degron}rrm3Δ$ was unviable (Figure 1B). We further characterized the terminal phenotypes of $sen1^{degron}rrm3Δ$ mutants. We first followed their cell cycle progression by fluorescence-activated cell sorting (FACS) profiles and tubulin staining by immunofluorescence. WT, $sen1^{degron}$, *rrm3Δ*, and $sen1^{degron}$ *rrm3Δ* cells were grown in YPG (permissive conditions), arrested in G1 in YPD (restrictive conditions), and released into S phase by maintaining the cells in YPD (Figure 1C). While WT, $sen1^{degron}$, and *rrm3Δ* strains progressed through the next cell cycle exhibiting comparable FACS profiles, the double mutants completed the bulk of DNA replication but arrested in G2/M (Figure 1C). Using tubulin and DAPI staining, we further characterized the cell cycle progression/arrest of the different strains (Figures 1C and 1D). While we observed normal metaphase to anaphase transitions and cell divisions in WT and single mutants, $sen1^{degron}rrm3Δ$ double mutants accumulated lagging chromosomes in the typical anaphase stage (Figure 1D).

$sen1^{degron}rrm3Δ$ mutants fail to complete replication termination

To visualize at the genome-wide level origin firing and fork progression we monitored DNA synthesis following bromodeoxyuridine (BrdU) incorporation and immunoprecipitation.[17] Cells were pre-synchronized in G1 and BrdU was added 30 min before the release into S phase in a fresh YPD medium containing BrdU and nocodazole to arrest cells after S phase (Figure S2A). All four strains were able to fire replication origins with comparable efficiency as shown by the appearance of BrdU peaks at the *ARS* genomic loci (Figure S2B). The number and the typical bimodal distribution of the BrdU peaks, as well as the extension of the relative clusters also being comparable in all strains, suggesting that the same origins were fired and that the bulk of DNA replication was not affected by *rrm3* and/or *sen1* mutations. Moreover, we did not observe unscheduled firing of additional origins in the mutant strains, which would be indicative of slow fork

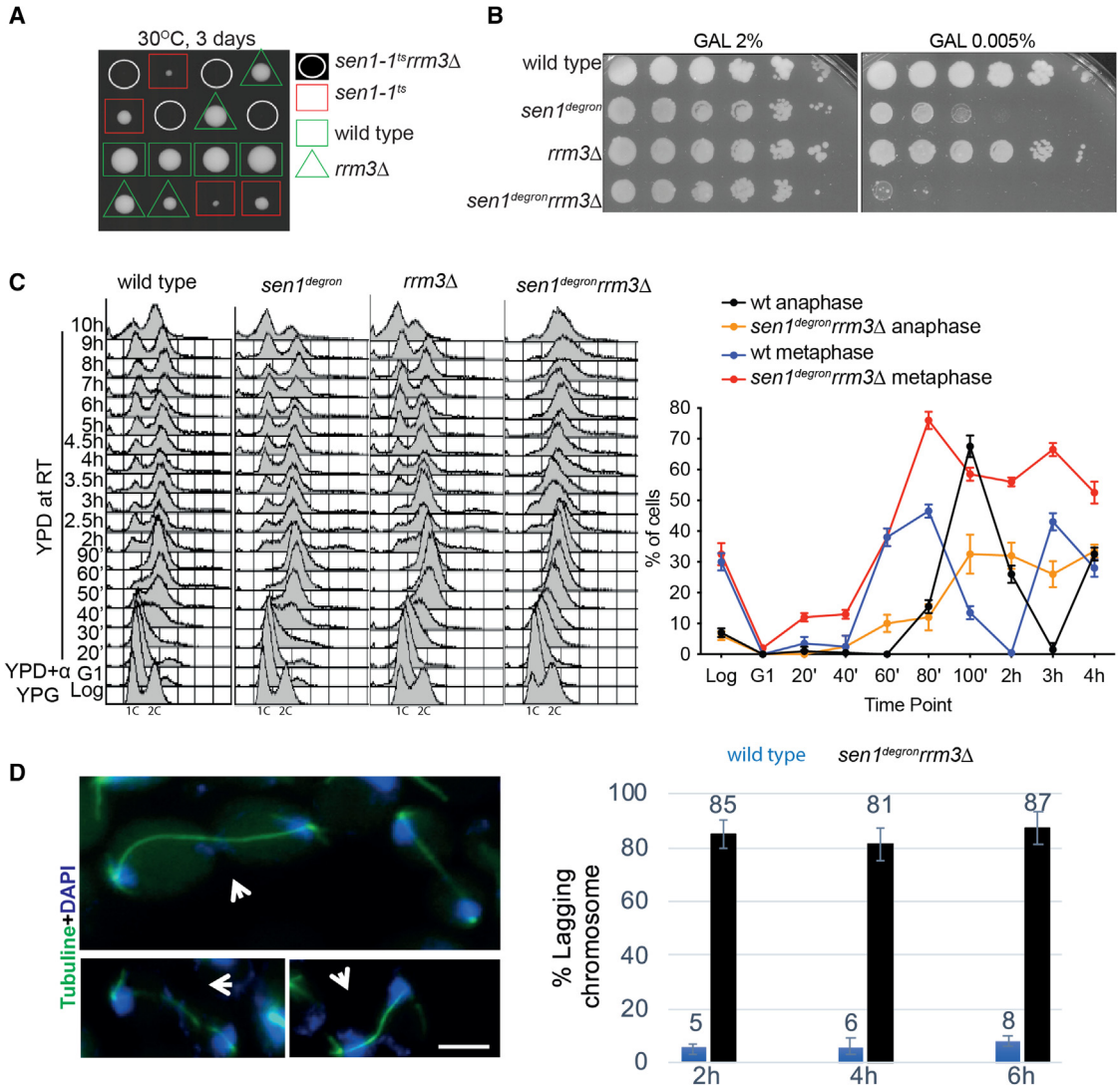

Figure 1. *sen1* and *rrm3* exhibit synthetic interactions and double mutants arrest in G2/M with lagging chromosomes

(A) Temperature-sensitive allele *sen1-1* and *rrm3Δ* crossed at 23°C and tetrad dissection viability scored at 30°C. White circles mark double-mutant (*sen1-1rrm3Δ*) genotype showing growth defect as synthetic interaction. Red square indicates *sen1-1*, green square indicates WT, and green triangle indicates *rrm3Δ*.

(B) Serial dilution-based spot assay for WT, *sen1*^{degron}, *rrm3Δ*, and *sen1*^{degron}*rrm3Δ* on YP + 2% raffinose plates having different amount of galactose 2% and 0.005%. Plates were kept at 28°C for 3 days and scanned.

(C) Log culture of WT, *sen1*^{degron}, *rrm3Δ*, and *sen1*^{degron}*rrm3Δ* grown in YPG (2% galactose) and arrested at G1 in YPD (2% glucose) medium. Cells were released from alpha factor and samples were collected at indicated time points and analyzed using propidium iodide (PI) staining and FACS profiling for 10 h. Cell cycle progression followed with immunofluorescence (IF) using anti-tubulin antibody and DAPI. The percentage of metaphase and anaphase cells in WT and double-mutant *sen1*^{degron} *rrm3Δ*, indicated as course of time after release from G1. Metaphase and anaphase cells were counted and plotted as the percentage of total cells (y axis) against time points (x axis). At each time point, more than 200 cells scored from two independent experiments and mean ± SD plotted.

(D) Lagging chromosomes scored with DAPI and tubulin staining. Representative IF images of tubulin (green) and DAPI (blue) staining of double-mutant *sen1*^{degron} *rrm3Δ* strain at 4-h time point after release from G1 (scale bar, 2 μm). White arrows indicate DAPI-positive signal as lagging chromosomes along tubulin staining axis. The left panel shows a bar graph plot of the percentage of anaphase cells carrying lagging chromosome in WT and *sen1*^{degron}*rrm3Δ* strains at indicated time points. More than 200 cells scored from two independent experiments and mean ± SD plotted.

progression or extensive fork collapse. We then analyzed the kinetics of appearance and disappearance and the quality of the replication intermediates at *ARS305* using the 2D gel technique[41] (Figure S2C). WT, *sen1*^{degron}, *rrm3Δ*, and *sen1*^{degron}*rrm3Δ* cells were pre-synchronized in G1 and released into S phase. All four strains accumulated bubble intermediates at 20 min after release from G1 with comparable efficiency. The bubble structures represent the typical intermediates generated by origin firing, thus implying that single and double mutants are proficient in origin firing. The replication intermediates progressively disappeared from the restriction fragment containing *ARS305* with comparable kinetics in all four strains, indicating

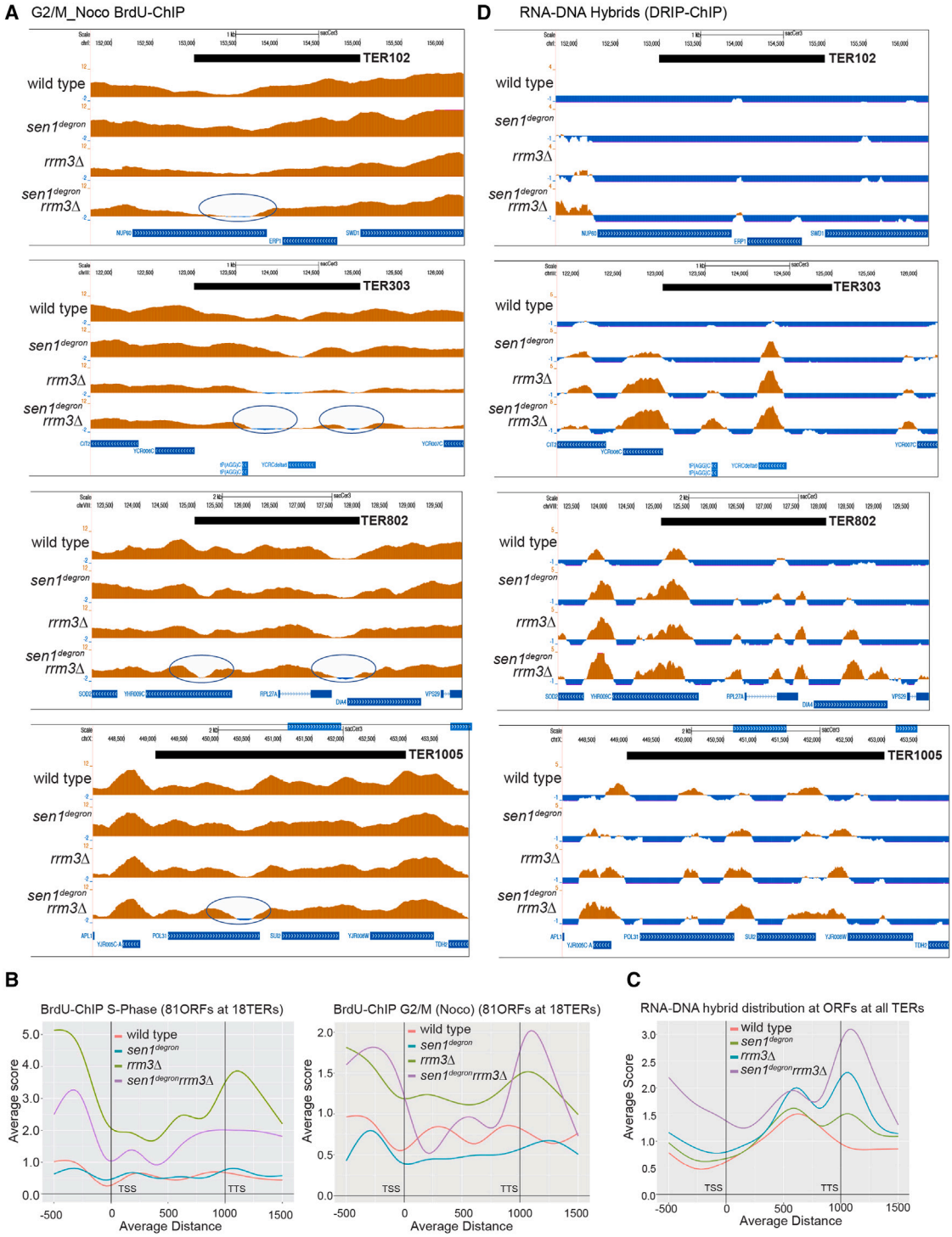

Figure 2. *sen1*^{degron}*rrm3Δ* mutants fail to complete replication termination and accumulate RNA-DNA hybrids at *TER*s

(A) WT, *sen1*^{degron}, *rrm3Δ*, and *sen1*^{degron}*rrm3Δ* were released from G1 into S phase in YPD + BrdU medium and arrested in G2/M using nocodazole. Samples were analyzed by BrdU-ChIP as described.[3] Representative genome browser snaps are shown for *TER102*, *TER303*, *TER802*, and *TER1005*. Blue circles indicate genomic regions defective in BrdU incorporation in double mutants.

(B) Metaplot analysis of average BrdU incorporation at 18 *TER*s transcriptionally active during S phase and G2/M (nocodazole arrested cells). BrdU-immunoprecipitation (IP) signal average binned around 81 ORFs and represented as average score around gene boundaries TSS and TTS for WT, *sen1*^{degron}, *rrm3Δ*, and *sen1*^{degron}*rrm3Δ*. The average score value difference between gene body and gene boundaries represents polar fork pausing or stalling.

(legend continued on next page)

that forks moved far from the *ARS305* locus with similar speed. We did not observe aberrant replication intermediates in the mutant strains. We therefore conclude that *sen1*^{degron}, *rrm3Δ*, and *sen1*^{degron}*rrm3Δ* mutants are not impaired in origin firing or fork progression per se.

We then visualized replicon fusion by following BrdU incorporation and immunoprecipitation and monitoring fork progression at late time points.[3] We were able to visualize replication fork fusion across *TER*s localized in between early firing origins with inter-origin distance up to 25 kb with high confidence. Seventy-one *TER*s have been mapped with this approach[3]; 23 out of 71 *TER*s have an inter-origin distance between 10 and 25 kb and, under our experimental conditions, were replicated in the WT background (Table S1); 22 of these *TER*s accumulated unreplicated gaps in *sen1*^{degron}*rrm3Δ* mutants (Table S1). Examples of replicon fusions in WT, *sen1*^{degron}, *rrm3Δ*, and *sen1*^{degron}*rrm3Δ* cells are shown (Figure 2A). At *TER102*, WT, *sen1*^{degron}, and *rrm3Δ* cells completed replication, while the double mutants accumulated one unreplicated gap. At *TER303*, while WT cells were able to complete replication, single mutants exhibited a delayed termination; the inability to complete replication was enhanced in the double mutants as shown by the accumulation of unreplicated gaps. At *TER802* and *TER1005*, WT and single mutants replicated across the *TER* zone while double mutants accumulated unreplicated gaps. The inability of *sen1*^{degron}*rrm3Δ* cells to complete replicon fusion at *TER*s reflected their failure to replicate across RNPII-transcribed genes within *TER*s as shown by a meta-analysis performed in BrdU chromatin immunoprecipitation (ChIP) experiments on 81 highly transcribed genes within 18 *TER*s (Figure 2B). During S phase, WT and *Sen1*^{degron} cells behaved similarly, while *rrm3Δ* and *Sen1*^{degron} *rrm3Δ* accumulated BrdU peaks at gene boundaries. We note that *rrm3Δ* cells in S phase already exhibit aberrant termination intermediates.[3] In G2, double mutants failed to complete termination, while all the other strains were able to incorporate BrdU at *TER*s, implying that, specifically in double mutants, both HD and CD forks (Figure S2D) failed to replicate across transcribed units at *TER*s.

sen1^{degron}*rrm3Δ* mutants accumulate RNA-DNA hybrids at *TER*s

We previously showed that *sen1*^{degron} and *rrm3Δ* exhibited a genome-wide RNA-DNA hybrid accumulation at all open reading frames (ORFs).[10] Based on those findings, we speculated that *sen1*^{degron}*rrm3Δ* double mutants might also be unable to suppress RNA-DNA hybrid accumulations at *TER*s. WT, *sen1*^{degron}, *rrm3Δ*, and *sen1*^{degron}*rrm3Δ* were released from G1into S phase for 45 min. In WT cells, the hybrids accumulated within the coding regions of the ORFs, as shown[10] (Figure 2C). We found aberrant hybrid accumulations in *sen1*^{degron} and *rrm3Δ* mutants at transcription termination sites (TTSs), although in *rrm3Δ* mutants the phenotype was more pronounced (Figure 2C). The double-mutant combination exhibited higher accumulation of hybrids at TTSs, and, at a lower level, also at transcription start sites (TSSs) (Figure 2C). Examples of hybrid accumulation at *TER*s *102*, *303*, *802*, and *1005* in WT, *sen1*^{degron}, *rrm3Δ*, and *sen1*^{degron}*rrm3Δ* cells are shown (Figure 2D). In all cases, single and double mutants exhibited aberrant hybrid accumulation, compared to WT cells, although the effects in single mutants were less pronounced compared to double mutants.

sen1^{degron} and *sen1*^{degron}*rrm3Δ* mutants accumulate RNPII at *TER*s and telomeres

We investigated whether the accumulation of RNA-DNA hybrids following Rrm3 ablation and/or Sen1 depletion also caused the accumulation of the RNPII catalytic subunit. WT, *sen1*^{degron}, *rrm3Δ*, and *sen1*^{degron}*rrm3Δ* were released from G1 into S phase and samples were taken at 45 min (Figure 3). Anti-Rpb1 antibodies were used to visualize the genome-wide distribution of the RNPII catalytic subunit by ChIP sequencing (ChIP-seq). Metanalysis performed at all ORFs showed that Rpb1 distributed along the coding regions accumulated preferentially in the proximity of TTSs (Figure S3A). We failed to observe significant differences between the four strains at the level of metanalysis (Figure S3A). However, when we analyzed in detail Rpb1 distribution within *TER*s, we found that specifically *sen1*^{degron} and *sen1*^{degron}*rrm3Δ* mutants accumulated Rpb1 at those genes transcribed within *TER*s (Figures 3A and 3B). We conclude that Sen1 plays a major role in preventing the accumulation of RNPII at those transcribed units clashing with replication forks at *TER*s. Hence, while both *sen1* and *rrm3* mutants accumulate hybrids, only in the case of *sen1* does hybrid accumulation correlate with RNPII accumulation. We reasoned that the synthesis of the leading strands of CD forks would stall in front of trapped RNPII complexes and replication across RNPII-transcribed genes within *TER*s would have to rely on the action of Rrm3 traveling on the lagging strands of the approaching HD forks (Figure S3B). This would not be possible in *sen1*^{degron}*rrm3Δ* mutants. In this view, a logical expectation would be that, in *sen1*^{degron} mutants, those subtelomeric forks approaching the last CD transcribed genes would also exhibit an aberrant accumulation of RNPII. We found that specifically *sen1*^{degron} and *sen1*^{degron}*rrm3Δ* mutants accumulated Rpb1 at telomeric regions when forks encounter transcribed genes in a CD way (Figure 3C and Table S2).

Sen1 and Rrm3 suppress chromosome fragility at *TER*s and telomeres

Fragile sites are chromosomal loci characterized by an intrinsic fragility that is expressed in certain genetic backgrounds and cancer cells following replication stress.[42–44] Termination zones exhibit all the potentially genotoxic features of fragile sites due to the significant topological stress resulting from replication fork fusion and the clash with transcription units. In fact, 36 out of 71 *TER*s have been classified as fragile sites[15] (Table S1). We then used copy number variation (CNV) analysis to address whether *sen1*^{degron}*rrm3Δ* cells exhibit *TER* fragility (Figure S3C).

(C) Genome-wide RNA-DNA hybrid analysis was performed by DRIP-ChIP. WT, *sen1*^{degron}, *rrm3Δ*, and *sen1*^{degron}*rrm3Δ* strains were released in S phase in YPD and harvested at 45 min for RNA-DNA hybrid IP and microarray hybridization. Metaplot analysis showing average score at 297 ORFs at all *TER*s.
(D) Representative genome browser profiles of aberrant DNA-RNA hybrid accumulation at transcriptionally active *TER102*, *TER303*, *TER802*, and *TER1005* in WT, *sen1*^{degron}, *rrm3Δ*, and *sen1*^{degron}*rrm3Δ*.

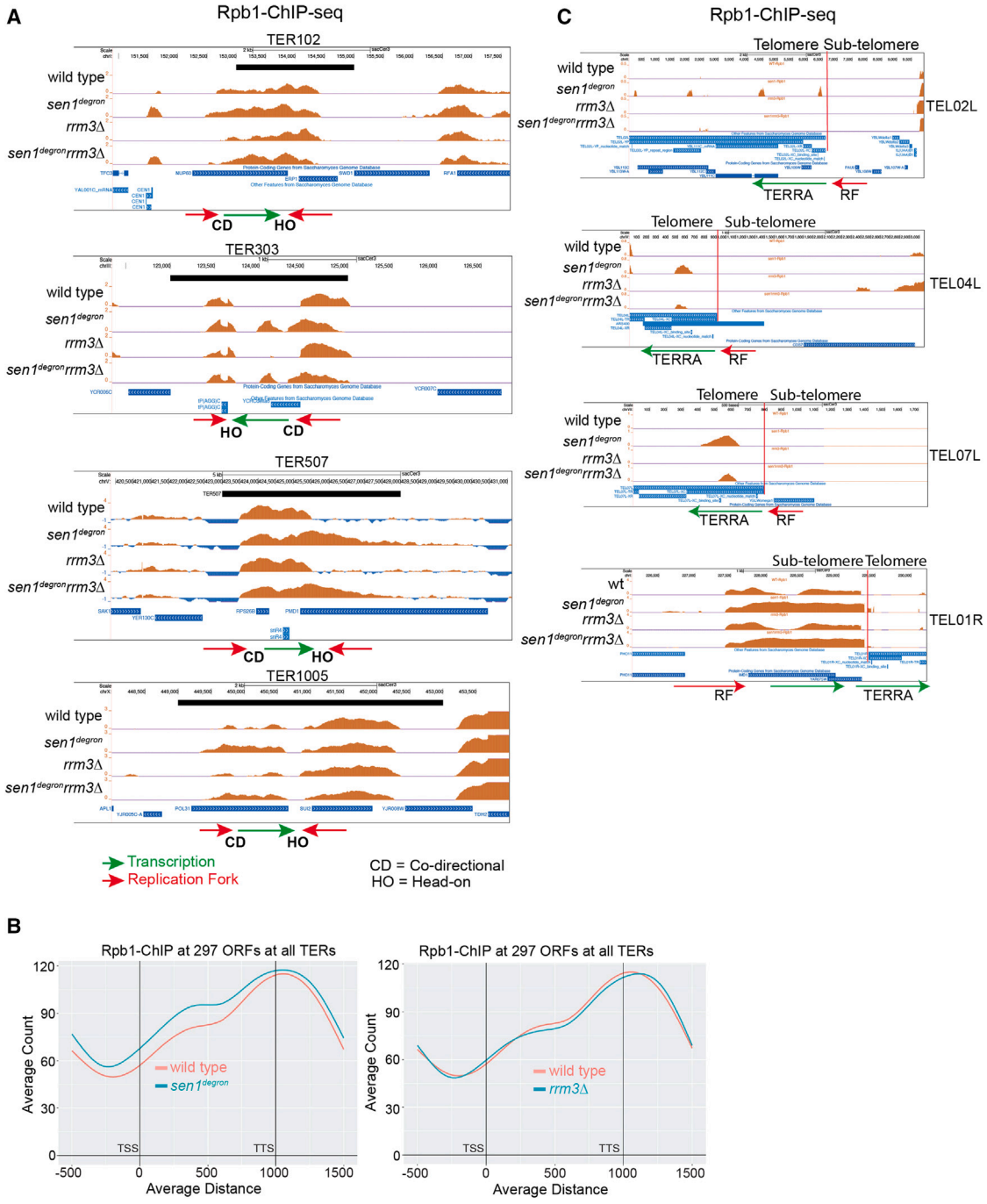

Figure 3. *sen1*^{degron} and *sen1*^{degron}*rrm3Δ* mutants accumulate RNPII at *TER*s and telomeres

(A) ChIP-seq analysis of genome-wide RNPII (Rpb1) distribution using anti-Rpb1(8WG16) antibody. Log cells were arrested in G1 and released into S phase; samples were harvested at 45 min. Representative genome browser profile showing Rpb1 accumulation in WT, *sen1*^{degron}, *rrm3Δ*, and *sen1*^{degron}*rrm3Δ* at *TER102*, *TER303*, *TER507*, and *TER1005*. ORFs were marked with green arrow and their relative orientation with respect to the converging replication fork (red arrow) is shown as CD or HD orientation.

(B) Average count metaplot for RNPII ChIP-seq data during S phase at ORFs at *TER*s. WT, *sen1*^{degron}, *rrm3Δ*, and *sen1*^{degron}*rrm3Δ* cells were released from G1 and into S phase to map RNPII genome-wide occupancy as shown in Figure S3. Here plotted as average score at 297 ORFs at all *TER*s indicating Sen1-dependent RNPII accumulation compared to *rrm3Δ*.

(C) Rpb1-ChIP-seq profiles at telomeres (*TEL02L*, *TEL04L*, *TEL07L*, and *TEL01R*). Green arrows indicate the direction of telomeric transcript TERRA from the subtelomeric region and the red arrow indicates terminal replication forks encountering TERRA transcript in a CD manner. Representative genome browser profile showing Rpb1 accumulation chromosomal ends in WT, *sen1*^{degron}, *rrm3Δ*, and *sen1*^{degron}*rrm3Δ*.

We released WT and *sen1^{degron}rrm3Δ* mutants from G1 into S phase in the presence of nocodazole for 3 h. The samples were then processed by CNV. We found that 30 *TER*s exhibited amplifications/deletions (Table S3). Moreover, we found that, out of 32 telomers, 11 exhibited significant CNV changes (Table S3).

Aberrant Top1 and Top2 activities contribute to topological abnormalities in *sen1^{degron}*, *rrm3Δ*, and sen1^{degron}rrm3Δ mutants

The formation of RNA-DNA hybrids is influenced by the chromatin topological state.[6,45] We therefore tested whether the failure to complete replication and the accumulation of RNA-DNA hybrids at *TER*s in *sen1^{degron}rrm3Δ* mutants would reflect topological abnormalities. We compared the genome-wide supercoil state of WT, *sen1^{degron}*, *rrm3Δ*, and *sen1^{degron} rrm3Δ* mutants (Figure 4). We analyzed the supercoil state at all ORFs and found that *sen1^{degron}*, *rrm3Δ*, and *sen1^{degron}rrm3Δ* mutants exhibited a dramatic and comparable reduction of negative supercoil and a concomitant increase of positive supercoil, compared to WT cells (Figures 4A and 4B). The accumulation of positive supercoil was more prominent in *sen1^{degron}rrm3Δ* mutants compared to single mutants. Since Sen1 and Rrm3 facilitate RNPII and fork advance, respectively, we reasoned that these two helicases may contribute to coordinate transcription and replication progression with Top1 and Top2 activities. These data imply that the reduction of negative supercoiling per se does not prevent termination in single mutants. We therefore tested whether the aberrant supercoil distributions in *sen1^{degron}*, *rrm3Δ*, and *sen1^{degron}rrm3Δ* mutants were due to unrestrained Top1 and/or Top2 activities. We found that Top1 ablation rescued the reduction of negative supercoil in *sen1^{degron}* and *sen1^{degron}rrm3Δ* mutants but, instead, enhanced it in *rrm3Δ* mutants (Figures 4C, 4D, and 4E). We analyzed the genome-wide Top1 distribution in the different strains and did not find significant differences (Figure 4F). However, specifically at those ORFs located within the TERs, Top1 was limiting in *rrm3Δ* and, at a lower extent, in *sen1^{degron}* mutants (Figure 4G). Moreover, *sen1^{degron}rrm3Δ* double mutants resembled *sen1^{degron}* cells. Altogether these observations suggest that the aberrant accumulation of positive supercoiling in *rrm3Δ* mutants is due the lack of Top1 and, likely, to an unscheduled Top2 activity that compensates for Top1 deficiency. Moreover, the finding that Top1 is no longer limiting in *sen1^{degron}rrm3Δ* further suggests that Sen1 plays an active role in displacing Top1 from *TER*s in the absence of Rrm3. We then introduced the *top2-1* mutation in *sen1^{degron}*, *rrm3Δ*, and *sen1^{degron}rrm3Δ* strains (Figures 4H–4J). We found that *top2-1* rescued the negative supercoil reduction in all mutant strains, indicating that Top2 contributes to convert negative supercoil into positive when Sen1 and/or Rrm3 are defective. We conclude that, in the absence of functional Sen1 and Rrm3, Top1 and Top2 exhibit aberrant activities causing topological abnormalities.

Chromosomal fragments that fail to complete replication do not to migrate on pulsed-field gel electrophoresis (PFGE).[3] We previously used the EagI genomic fragment of chromosome III harboring *ARS305*, *TER301*, *ARS306*, *TER302*, and *ARS307* (Figure S4A) to characterize replication termination in different genetic backgrounds.[3] In WT, *sen1^{degron}*, and *rrm3Δ* strains, CHRIII and the EagI genomic fragment were retained in the wells at 1 h after release from G1 and, later on, when replication was completed, they migrated normally in the gels. Conversely, in *sen1^{degron}rrm3Δ* cells, CHRIII and the EagI genomic fragment remained entrapped in the wells also at later time points, likely due to incomplete replication termination (Figure S4B). We found that, in *sen1^{degron}rrm3Δ* double mutants, the gel retention of the EagI genomic fragment was partially rescued by introducing the *top2-1* mutation, again suggesting that Top2 activity contributes to the aberrant termination events owing to Sen1 and Rrm3 defects (Figure S4C).

We then analyzed the topological context of telomeric regions in WT, *sen1^{degron}*, *top2-1*, and *sen1^{degron} top2-1* mutants. In WT cells, out of 32 telomeres, 17 are longer than 1 kb and are characterized by large over-wound modules flanking small negatively supercoiled regions (Table S2 and Figure S4D). The remaining 15 short telomeres exhibit heterogeneous topological contexts (Table S2). In *sen1^{degron}* mutants, all 17 long telomeres, as well as the short *Tel01R* telomere, are heavily positively supercoiled with no obvious under-wound regions. *Top2-1* and *sen1^{degron} top2-1* mutants display a topological telomeric profile similar to WT cells (Table S2 and Figure S4D). We conclude that the aberrant positive supercoil accumulation in *sen1^{degron}* telomeres is caused by unrestrained Top2 activity.

sen1^{dg}rrm3Δ strain accumulates aberrant replication termination intermediates

We used the *in vivo* psoralen-mediated DNA inter-strand cross-linking technique coupled to low angle rotary shadowing and transmission electron microscopy (EM) to analyze the fine ultrastructure of the DNA replication intermediates accumulating in WT and *sen1^{degron}rrm3Δ* cells.[46] WT, *sen1^{degron}*, *rrm3Δ*, and *sen1^{degron}rrm3Δ* strains were pre-synchronized in nocodazole and released in the presence of alpha factor to arrest them in G1 in the next cell cycle. Sen1 shutoff was induced during the alpha factor treatment. Cells were then released into S phase at 23°C and samples were collected at 45 min (middle S phase) (Figure S5A). In WT cells, 89% of RIs were normal forks in the classic three-branch Y-shaped conformation (Figures 5A and 5B), 6% were termination structures in the typical double-Y conformations (Figures S5B, 5A, and 5C), 2% were X-shaped structures resembling reversed forks (Figures S5B, 5A, and 5D), and 3% were forks with short gaps at the branching point in one of the two replicated daughter chains (FiguresS5B, 5A, and 5B). *sen1^{degron}* and *rrm3Δ* mutants exhibited a reduction in the relative number of normal forks (87% and 78%, respectively) and an increase of termination intermediates (11% and 17%, respectively). *sen1^{degron}rrm3Δ* mutants exhibited 74% normal forks, 19% termination intermediates, 4% reversed forks, and 3% of gapped forks. We noticed that, specifically in double-mutant cells, out of the termination intermediates, 69% were in the double-Y conformation (Figures S5B), 17% were characterized by two fully converged forks (Figures S5B), and 14% by a subclass of aberrant DNA replication termination intermediates carrying single-strand DNA (ssDNA) stretches at the branching points of one of the two converging forks generating the DNA replication termination center (Figures S5B and 5E). The average length of the gaps was 399 nt (Figure S5C). We note that the gaps

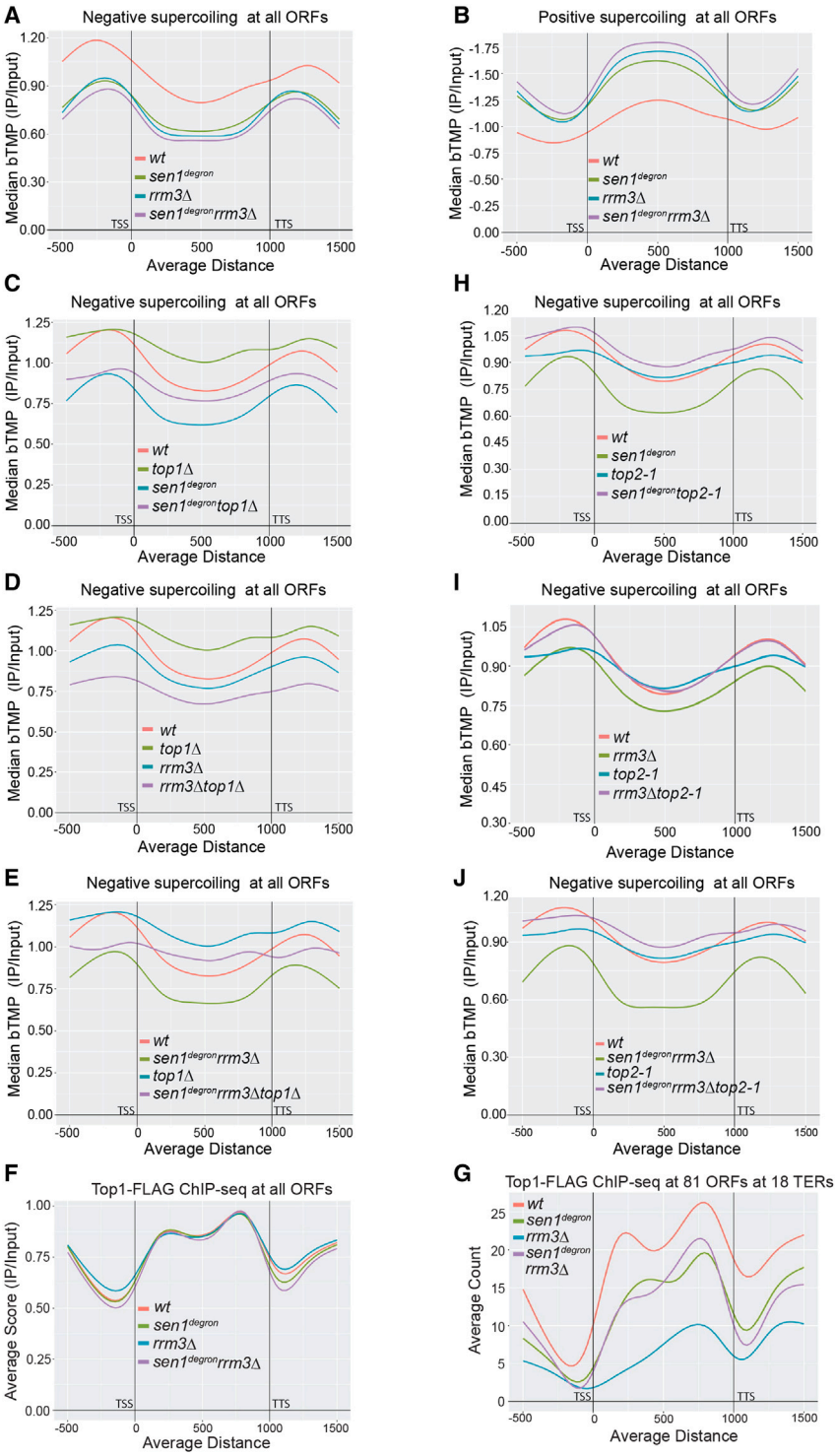

Figure 4. Unrestrained Top1 and Top2 activities contribute to topological abnormalities in *sen1*^{degron}, *rrm3Δ*, and *sen1*^{degron}*rrm3Δ* mutants

(A) Modulation of negative supercoiling at gene bodies and boundaries at all ORFs. WT, *sen1*^{degron}, *rrm3Δ*, and *sen1*^{degron}*rrm3Δ* were released from G1 into S phase and harvested at 40-min time point for bTMP-seq analysis. Data represented as metaplots using median bTMP (IP/input) at 6,706 genes. At the x axis, all ORFs binned in 1,000 bp and flaking areas as ±500 bp. At the y axis, median bTMP (IP/input) is represented and indicates an overall reduction in negative supercoiling in *sen1*^{degron}, *rrm3Δ*, and *sen1*^{degron}*rrm3Δ* compared to WT.

(B) Accumulation of positive supercoiling at all ORFs. The same samples as in (A) were analyzed for positive supercoiling and represented as median bTMP (IP/input) at 6,706 genes. Extent of bTMP intercalation (positive peaks on ChIP-seq) scored as negative supercoiling and exclusion of bTMP intercalation (negative peaks on ChIP-seq) scored as positive supercoiling. Metaplot as negative median bTMP (IP/input) for positive supercoiling indicates increased positive supercoiling in *sen1*^{degron}, *rrm3Δ*, and *sen1*^{degron}*rrm3Δ* compared to WT.

(C) bTMP-seq data represented as median bTMP (IP/input) in WT, *sen1*^{degron}, *top1Δ*, and *sen1*^{degron}*top1Δ* at all ORFs. Log cells moved from galactose to glucose at room temperature and harvested after 2 h for bTMP-seq.

(D) Median bTMP (IP/input) for bTMP-seq data for WT, *rrm3Δ*, *top1Δ*, and *rrm3Δtop1Δ*. Log cells moved from galactose to glucose at room temperature and harvested after 2 h for bTMP-seq.

(E) Median bTMP (IP/input) of bTMP-seq dataset in WT, *sen1*^{degron}*rrm3Δ*, *top1Δ*, and *sen1*^{degron}*rrm3Δtop1Δ*. Log cells moved from galactose to glucose at room temperature and harvested after 2 h for bTMP-seq.

(F) Top1 occupancy during S phase in WT, *sen1*^{degron}, *rrm3Δ*, and *sen1*^{degron}*rrm3Δ* strains. Endogenous Top1 tagged with 10xFLAG in WT, *sen1*^{degron}, *rrm3Δ*, and *sen1*^{degron}*rrm3Δ* strains and cells were released from G1 to S phase for Top1 chromatin binding using ChIP-seq. Genome-wide average score shown at all ORFs in WT, *sen1*^{degron}, *rrm3Δ*, and *sen1*^{degron}*rrm3Δ* strains for Top1-FLAG ChIP-seq.

(G) Average count metaplot for Top1-FLAG ChIP-seq at 81 ORFs at 18 TERs in WT, *sen1*^{degron}, *rrm3Δ*, and *sen1*^{degron}*rrm3Δ* strains.

(H) Median bTMP (IP/input) of bTMP-seq dataset for WT, *sen1*^{degron}, *top2-1*, and *sen1*^{degron}*top2-1*. Cells were moved to YPD and later at semi-permissive temperature for the *Top2* mutation (32°C for 1 h).

(I) Median bTMP (IP/input) of bTMP-seq dataset in WT, *rrm3Δ*, *top2-1*, and *rrm3Δ top2-1*. Cells were moved to YPD and later at semi-permissive temperature for the *Top2* mutation (32°C for 1 h).

(J) Median bTMP (IP/input) of bTMP-seq dataset in WT, *sen1*^{degron}*rrm3Δ*, *top2-1*, and *sen1*^{degron}*rrm3Δtop2-1*. Cells were moved to YPD and later at semi-permissive temperature for the *Top2* mutation (32°C for 1 h). Experiments described in (A) and (B) are from the same experiment. Experiments described in (C)–(E) are from the same experiment. Experiments described in (H)–(J) are from the same experiment. Experiments described in (F) and (H) are from the same experiment.

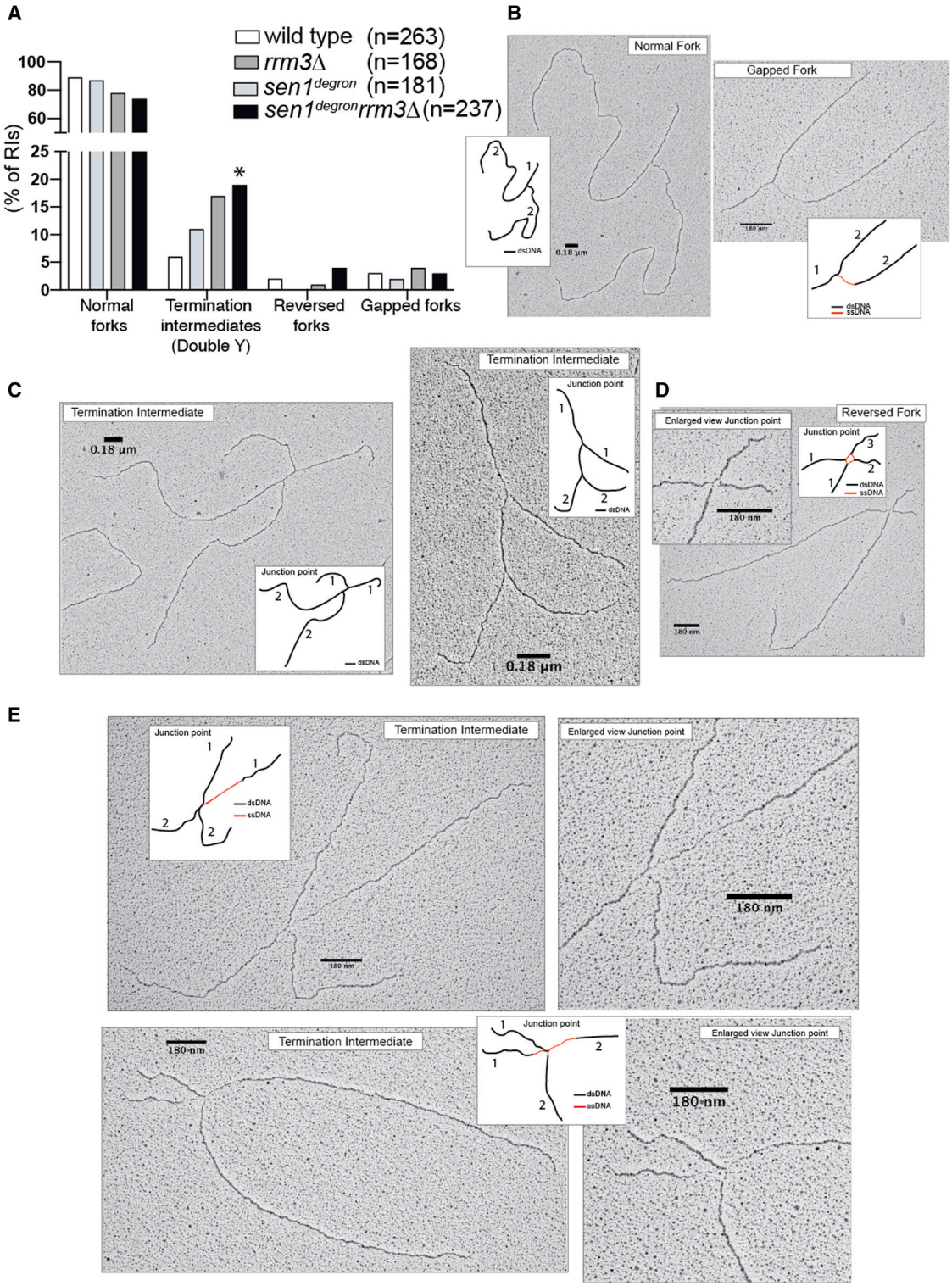

Figure 5. *sen1*^{degron}*rrm3Δ* accumulates aberrant replication termination intermediates

(A) Histogram showing the percentages of DNA replication intermediates subjected to *in vivo* psoralen-mediated DNA inter-strand cross-linking and isolated from the strains with the indicated genotypes. Normal forks, double-Y (DNA replication termination intermediates), reversed forks (and other X-shaped molecules), and gapped forks (defined as forks with more than 200 nt of ssDNA localized at the fork branching point) are shown. Yeast strains were released from G1 into S phase at 23°C and harvested after 45 min from the release (mid-S phase). Numbers (n) of molecules analyzed for WT (N = 2, n = 263), *sen1*^{degron} (N = 1, n = 181), *rrm3Δ*

(legend continued on next page)

in the termination structures did not exhibit secondary structures, despite the *in vivo* psoralen cross-linking treatment that would preserve them. This implies that the denatured conformation of the ssDNA tracts observed in our analysis derives from intermediates that *in vivo* prevent the formation of secondary structures. We then used the denaturing spreading technique[47,48] to investigate in more detail the structural features of the aberrant DNA replication termination intermediates isolated in the double-mutant *sen1*^{degron}*rrm3Δ*. We note that psoralen is unable to crosslink the DNA wrapped around the nucleosomes and acts specifically on the linker DNA. Hence, following denaturation, it is possible to visualize nucleosomal bubbles. We found that long ssDNA stretches were indeed present at the branching point of one of the two converging forks creating the DNA replication termination center and that the duplex chains in the termination structures, including those duplex tracts opposite to the ssDNA gaps, were organized into nucleosome bubbles (Figure S5D). We also performed an analogous analysis at 100 min after release from G1, when cells are in late S phase (Figures S5, S5E, and S5F). We found that WT cells exhibited 85% normal forks, 12% termination structures, and 3% reversed forks. We no longer observed gapped forks. *sen1*^{degron}*rrm3Δ* mutants exhibited a significant accumulation of termination structures (25%) and reversed forks (15%). Within the termination structures, we still observed ssDNA gaps at those termination structures characterized by fully converged forks, although the average size was reduced to 259 nt (Figure S5C). In double-mutant cells, we rarely visualized termination intermediates with both converged forks into a reversed fork conformation (Figure S5G). We conclude from these observations that, while in WT cells termination structures are quite rare, likely reflecting their rapid turnover, *sen1*^{degron} and *rrm3Δ* mutants accumulate termination intermediates, likely reflecting a delay in replication termination. Moreover, our data suggest that *sen1*^{degron}*rrm3Δ* mutants fail to complete fork fusion and accumulate aberrant termination structures and, later on, reversed forks.

DISCUSSION

We showed that replication termination relies on the coordinated action of two specialized helicases, Rrm3 and Sen1, that assist converging forks when encountering transcription units HD or CD, respectively. While WT cells can deal with HD and CD collisions between replication and transcription, in the absence of functional Rrm3 and Sen1, replicons fail to fuse; this implies that no other helicase is able to substitute Rrm3 and Sen1 at termination. Rrm3 travels on DNA with the fork with a 3′ to 5′ polarity[19,22,23] and clashes with the 3′ end of nascent transcripts when forks encounter transcripts HD; Sen1 facilitates transcription termination by moving with a 5′ to 3′ polarity on nascent RNAs[49–51] and, therefore, travels codirectionally with leading strands. At *TER*s the two replication forks encounter the last transcription unit from opposite directions in HD and CD conformations. In the absence of one of the two helicases, termination can still be achieved as both *sen1* and *rrm3* mutants can eventually complete replicon fusion. However, telomeres represent an exception because their duplications rely on one terminal fork that has to reach the end of the chromosome and deal with subtelomeric transcription and topological constrains.[13,52] Sen1 plays a key role in mediating efficient replication completion at telomeres when terminal forks encounter the last subtelomeric transcript codirectionally. The inability of *sen1* mutants to remove RNPII at those transcripts positioned CD with terminal forks cannot be rescued by Rrm3 (Figure 3B) and generates the ideal context to uncouple leading and lagging strand synthesis: trapped RNPII would block leading-strand synthesis of terminal forks but not necessarily lagging-strand synthesis (Figure S6A). Notably, in *sen1* mutants, the 3′ ends of CD transcripts likely cannot be used to prime re-start replication events as they would be masked by trapped RNPII complexes. HD forks might also undergo leading-lagging uncoupling in the absence of Rrm3 but, in this case, the transcripts would specifically block lagging-strand progression, while the leading strand would continue the synthesis (Figure S6A). This scenario may account for the replication pausing phenotype of *rrm3* mutants.[53]

Our data suggest that Rrm3 and Sen1 helicases coordinate replisome and transcriptome movements, respectively, with Top1 and Top2 activities. The clash between forks and transcribed units implies that fork-associated Top1 and Top2 (replicative Top1 and Top2) must encounter the fractions of Top1 and Top2 associated with gene loops (transcription-related Top1 and Top2).[54] Since replicative and transcription-related topoisomerases can process the same supercoil substrates, their activities must be properly coordinated and restrained in order to avoid aberrant topological events.[54] The finding that *rrm3* and *sen1* mutants exhibit abnormal topological profiles due to aberrant Top1 and Top2 activities implies that Rrm3 and Sen1 helicases contribute, indirectly, to the topological organization of chromosomes. Advancing replisomes rotate, generating positive supercoil in front of the fork and behind the forks through the formation of precatenanes.[4] Most likely, replicative Top1 resolves the positive supercoil in front of the fork, while Top2 resolves precatenation behind the fork.[4,7] When HD and CD forks encounter gene loops (Figures S6B and 6A), first they have to deal with negatively supercoiled gene boundaries in a cruciform conformation.[10] A possibility is that replicative topoisomerases

(N = 1, n = 168), and *sen1*^{degron}*rrm3Δ* (N = 2, n = 237). Asterisk (*) indicates a sub-fraction of DNA replication termination intermediates (double-Y structures) carrying ssDNA stretches on the daughter strands of the two converging forks creating the DNA replication termination center (see also E).

(B) Representative transmission electron microscopy (TEM) images of a normal fork and a gapped fork along with graphical schemes of the molecules with double-stranded DNA (dsDNA) (black), ssDNA (red), and branches of the molecules with the same length labeled with the same number.

(C) Representative TEM images (along with graphical schemes) of double-Y DNA structures as examples of DNA replication termination intermediates.

(D) Representative TEM image of a reversed fork and enlarged view of the fork branching point indicating the presence of a single Holliday junction-like structure carrying ssDNA as schematized in the graphical illustration.

(E) Representative TEM images (along with graphical schemes) of DNA replication termination intermediates (double-Y molecules) harboring ssDNA stretches localized on the daughter strands of one (or two) converging forks creating the DNA replication termination center.

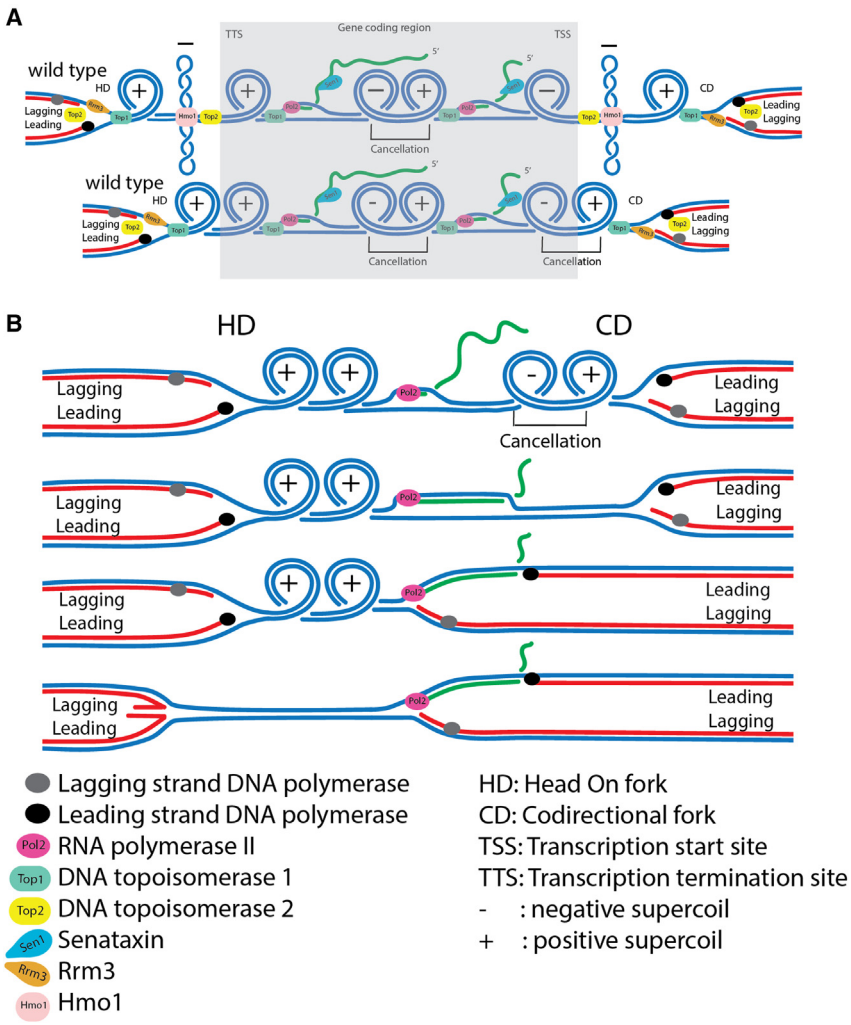

Figure 6. Schematic representations of the replication events occurring at *TERs*

(A) Linear representation of two converging forks encountering an active gene in WT cells. The gray area represents the gene body. HD and CD forks encounter the negatively supercoiled cruciform structures at the gene boundaries. Two transcription events are shown within the gene body, each of them generating a twin topological domain. See section "discussion" for details.

(B) Linear representation of two converging forks encountering an active gene in *sen1*^{degron}*rrm3Δ* cells. CD fork advancement would be facilitated by the attenuation of the topological stress in front of the fork as the positive supercoil generated by the advancing replisome would be canceled by the negative supercoil behind the transcribing RNPII. Due to Sen1 defects, CD forks would then pause in front of stable RNA-DNA hybrids generated by stalled RNPII complexes. HD forks would not be able to proceed due to the massive accumulation of positive supercoiling caused by unrestrained Top2 activity. Later on, the positive supercoiling in front of HD forks may actively promote fork reversal (see section "discussion" for details).

may contribute to resetting the gene loop architecture by processing gene boundaries.[54] Notably, both Top1 and Top2 can act on positive and negative supercoiling.[4,9,55] When forks engage in replication of actively transcribed coding regions the topological context changes (Figure 6A), HD collisions will accumulate positive supercoil in front of RNA polymerases and DNA polymerases; CD collisions, instead, will generate positive supercoil in front of the forks and negative supercoil behind the moving RNPII. Most likely, in the case of CD collisions, positive and negative supercoils will cancel each other, analogously to what happens between two RNPII complexes transcribing the same gene.[56] Hence, the topological stress generated by HD and CD forks is different. Our data show that, in *rrm3* mutants, Top2 contributes to the abnormal processing of negative supercoil both at gene boundaries and within coding regions. We speculate that, when forks reset the negatively supercoiled cruciform structures at gene boundaries, in the absence of Rrm3, unrestrained replicative Top2 and/or the fraction of Top2 dislodged by the base of the gene loops process the negative supercoil at gene boundaries and gene bodies. This scenario might be facilitated by the limiting amount of Top1 owing to *RRM3* ablation. One possibility is that pausing replisomes in *rrm3* mutants are less prone to rotate, and mutant cells cannot rely on Top1-mediated resolution of positive supercoil in front of the forks; this would be an ideal situation to unleash dangerous Top2 activities from the back of the forks.

In the case of *sen1* mutants, both Top1 and Top2 exhibit unrestrained activities resulting in negative supercoil resolution but, while Top2 causes a decrease in negative supercoil throughout the genes, Top1 acts specifically at the coding regions. We speculate that, in the absence of Sen1, RNPII slows down and no longer rotates[6]; this situation might delocalize Top1 from the front of transcription to the back, thus leading to the unscheduled processing of the negative supercoil of the twin topological domains. The unscheduled and unrestrained Top2 activity in *sen1* mutants may result from the defective Sen1 acting at transcription termination or at forks.[34] An analogous situation might also explain the aberrant accumulation of positive supercoil at telomeres in *sen1* mutants, owing to unrestrained Top2.

Replication and transcription pausing owing to *rrm3* or *sen1* mutations, respectively, together with the unrestrained Top1 and Top2 activities, can also account for the accumulation of RNA-DNA hybrids at *TER*s. In the absence of Rrm3, hybrids could form either at HD forks, due to leading-lagging uncoupling, and behind moving RNPII complexes due to aberrant processing of negative supercoil (Figure 6A). An important difference between *rrm3* and *sen1* mutants is that RNA-DNA hybrid accumulation in the absence of Rrm3 does not correlate with accumulation of stalled RNPII. However, also in the case of *rrm3* mutants, the 3′ ends of RNA-DNA hybrids unlikely can be engaged in

replication re-start events as they will clash with the 5′ ends of stalled lagging strands.

In *sen1rrm3* double mutants, the aberrant massive positive supercoil accumulation and the presence of persistent RNA-DNA hybrids prevent replicon fusion. The majority of the termination intermediates observed by EM in *sen1 rrm3* are characterized by large ssDNA gaps in a denatured conformation; these ssDNA tracts derive from intermediates that *in vivo* prevent the formation of secondary structures and likely represent the scars of RNA-DNA hybrids. We note that the experimental conditions used to visualize the replication intermediates by EM following psoralen cross-linking contemplate extensive RNAse treatment. During middle S phase, 52% of the termination intermediates are characterized by gaps located in the proximity of the branching point of one of the two converging forks. By the topological point of view, the aberrant accumulation of positive supercoil in *sen1rrm3* mutants would preferentially affect HD collisions as the positive supercoil in front of CD forks would be canceled by the negative supercoil on the back of the transcript[56] (Figure 6B). We speculate that the aberrant forks observed by EM generate in the absence of Sen1 during CD collisions due to leading-lagging uncoupling and that the simultaneous depletion of Rrm3 leads to the accumulation of stable RNA-DNA hybrids with RNPII trapped at the 3′ ends (Figure 6B). The topological complexity in front of HD forks not only would hamper their progression but would also create the ideal condition for fork reversal in a context in which extensive fork stalling may also destabilize replisome fork association; notably, fork reversal is induced by positive supercoil[57,58] and the branch migration of the reversed arm adsorbs the positive supercoil in front of the fork.[59] Based on the above considerations, we speculate that those rare termination intermediates with two reversed forks observed in *sen1rrm3* mutants (Figure S5H) may represent events in which the two converging forks clash HD with two transcripts.[3]

Altogether, our observations suggest that Rrm3 and Sen1 coordinate Top1 and Top2 activities when forks encounter transcription loops during replicon fusion and that the unrestrained activities of both topoisomerases in *rrm3* and *sen1* mutants can lead to aberrant topological events, accumulation of RNA-DNA hybrids, fragile site expression, and replication termination defects.

Limitations of the study

We predict that other, as-yet unknown factors may contribute to mediate the completion of replication, particularly at those genomic locations where replication termination takes place independently of transcription events. Moreover, it would be relevant to address how replication termination is achieved at telomeres and whether *TERRA* transcription contributes to the process. Finally, it is still unclear how replicative and transcription-related Top1 and Top2 are coordinated when forks encounter gene loops.

STAR★METHODS

Detailed methods are provided in the online version of this paper and include the following:

- KEY RESOURCES TABLE
- RESOURCE AVAILABILITY
  - Lead contact
  - Materials availability
  - Data and code availability
- EXPERIMENTAL MODEL AND STUDY PARTICIPANT DETAILS
  - Yeast growth conditions and cell cycle synchronizations
- METHOD DETAILS
  - FACs (fluorescence activated cell sorter) analysis
  - Immunofluorescence-IF staining
  - bTMP-seq
  - Protein-ChIP-seq
  - DRIP-chip
  - ChIP-seq data analysis
  - Microarray processing
  - *In-vivo* psoralen crosslinking of the DNA for EM analysis
  - Genomic DNA extraction (for EM, BrdU-chip and CNVs)
  - BrdU-chip
  - TEM analysis of replication intermediates
  - Pulse field gel electrophoresis (PFGE)
  - Copy number variation sequencing
  - CNV data analysis
- QUANTIFICATION AND STATISTICAL ANALYSIS

SUPPLEMENTAL INFORMATION

Supplemental information can be found online at https://doi.org/10.1016/j.celrep.2023.112747.

ACKNOWLEDGMENTS

We thank Kristina Havas (IFOM), Rodrigo Bermejo (CIB-CSIC-Spain), Hiroshi Arakawa (IFOM), and Ylli Doksani (IFOM) for critical reading of the manuscript and all the members of the M.F. laboratory for suggestions, as well as Chiara Lucca (IFOM) and Daniele Piccini (IFOM) for technical support. We thank IFOM ETS-Cogentech imaging facility for technical assistance (special thanks to Sara Barozzi). We thank Giuseppe Meroni (IFOM) for bTMP synthesis. We thank the Cogentech sequencing facility and Claudia Valli, Mirko Riboni, and Simone Minardi for support and technical assistance in microarray and DNA sequencing. R.C. was supported by Marie Curie Initial Training Network (ITN) (FP7 programme ADDRESS, project no. 316390). Work in M.F.'s laboratory is supported by grants from Associazione Italiana per la Ricerca sul Cancro, AIRC, Italy, and Ministero dell'Istruzione, dell'Università e della Ricerca (MIUR-PRIN-2015SJLMB9).

AUTHOR CONTRIBUTIONS

Supervision, M.F.; conceptualization, M.F. and R.C.; methodology, R.C.; software and genomics data analysis, M.A.; transmission EM image acquisition, M.G.; validation, R.C.; investigation, R.C. and J.N.B.; resources, G.L. and Y.J.A.; data curation, R.C. and M.A.; writing – original draft, M.F. and R.C.; visualization, M.F., R.C., and M.A.; funding acquisition, M.F. and R.C.

DECLARATION OF INTERESTS

The authors declare no competing interests.

Received: October 1, 2022
Revised: April 17, 2023
Accepted: June 20, 2023

REFERENCES

1. Srivatsan, A., Tehranchi, A., MacAlpine, D.M., and Wang, J.D. (2010). Co-orientation of replication and transcription preserves genome integrity. PLoS Genet. *6*, e1000810. https://doi.org/10.1371/journal.pgen.1000810.
2. Dewar, J.M., and Walter, J.C. (2017). Mechanisms of DNA replication termination. Nat. Rev. Mol. Cell Biol. *18*, 507–516. https://doi.org/10.1038/nrm.2017.42.
3. Fachinetti, D., Bermejo, R., Cocito, A., Minardi, S., Katou, Y., Kanoh, Y., Shirahige, K., Azvolinsky, A., Zakian, V.A., and Foiani, M. (2010). Replication termination at eukaryotic chromosomes is mediated by Top2 and occurs at genomic loci containing pausing elements. Mol. Cell. *39*, 595–605. https://doi.org/10.1016/j.molcel.2010.07.024.
4. Wang, J.C. (2002). Cellular roles of DNA topoisomerases: a molecular perspective. Nat. Rev. Mol. Cell Biol. *3*, 430–440. https://doi.org/10.1038/nrm831.
5. Ma, J., and Wang, M.D. (2016). DNA supercoiling during transcription. Biophys. Rev. *8*, 75–87. https://doi.org/10.1007/s12551-016-0215-9.
6. Bermejo, R., Lai, M.S., and Foiani, M. (2012). Preventing replication stress to maintain genome stability: resolving conflicts between replication and transcription. Mol. Cell. *45*, 710–718. https://doi.org/10.1016/j.molcel.2012.03.001.
7. Bermejo, R., Doksani, Y., Capra, T., Katou, Y.M., Tanaka, H., Shirahige, K., and Foiani, M. (2007). Top1- and Top2-mediated topological transitions at replication forks ensure fork progression and stability and prevent DNA damage checkpoint activation. Genes Dev. *21*, 1921–1936. https://doi.org/10.1101/gad.432107.
8. Wu, H.Y., Shyy, S.H., Wang, J.C., and Liu, L.F. (1988). Transcription generates positively and negatively supercoiled domains in the template. Cell *53*, 433–440.
9. Trigueros, S., and Roca, J. (2002). Failure to relax negative supercoiling of DNA is a primary cause of mitotic hyper-recombination in topoisomerase-deficient yeast cells. J. Biol. Chem. *277*, 37207–37211. https://doi.org/10.1074/jbc.M206663200.
10. Achar, Y.J., Adhil, M., Choudhary, R., Gilbert, N., and Foiani, M. (2020). Negative supercoil at gene boundaries modulates gene topology. Nature *577*, 701–705. https://doi.org/10.1038/s41586-020-1934-4.
11. Hashash, N., Johnson, A.L., and Cha, R.S. (2012). Topoisomerase II- and condensin-dependent breakage of MEC1ATR-sensitive fragile sites occurs independently of spindle tension, anaphase, or cytokinesis. PLoS Genet. *8*, e1002978. https://doi.org/10.1371/journal.pgen.1002978.
12. Tomáška, Ľ., Cesare, A.J., AlTurki, T.M., and Griffith, J.D. (2020). Twenty years of t-loops: A case study for the importance of collaboration in molecular biology. DNA Repair *94*, 102901. https://doi.org/10.1016/j.dnarep.2020.102901.
13. Ye, J., Lenain, C., Bauwens, S., Rizzo, A., Saint-Léger, A., Poulet, A., Benarroch, D., Magdinier, F., Morere, J., Amiard, S., et al. (2010). TRF2 and apollo cooperate with topoisomerase 2alpha to protect human telomeres from replicative damage. Cell *142*, 230–242. https://doi.org/10.1016/j.cell.2010.05.032.
14. Zhang, T., Zhang, Z., Li, F., Hu, Q., Liu, H., Tang, M., Ma, W., Huang, J., Songyang, Z., Rong, Y., et al. (2017). Looping-out mechanism for resolution of replicative stress at telomeres. EMBO Rep. *18*, 1412–1428. https://doi.org/10.15252/embr.201643866.
15. Song, W., Dominska, M., Greenwell, P.W., and Petes, T.D. (2014). Genome-wide high-resolution mapping of chromosome fragile sites in Saccharomyces cerevisiae. Proc. Natl. Acad. Sci. USA *111*, E2210–E2218. https://doi.org/10.1073/pnas.1406847111.
16. Kleckner, N., Zickler, D., Jones, G.H., Dekker, J., Padmore, R., Henle, J., and Hutchinson, J. (2004). A mechanical basis for chromosome function. Proc. Natl. Acad. Sci. USA *101*, 12592–12597. https://doi.org/10.1073/pnas.0402724101.
17. Bermejo, R., Capra, T., Jossen, R., Colosio, A., Frattini, C., Carotenuto, W., Cocito, A., Doksani, Y., Klein, H., Gómez-González, B., et al. (2011). The replication checkpoint protects fork stability by releasing transcribed genes from nuclear pores. Cell *146*, 233–246. https://doi.org/10.1016/j.cell.2011.06.033.
18. Kumar, A., Mazzanti, M., Mistrik, M., Kosar, M., Beznoussenko, G.V., Mironov, A.A., Garrè, M., Parazzoli, D., Shivashankar, G.V., Scita, G., et al. (2014). ATR mediates a checkpoint at the nuclear envelope in response to mechanical stress. Cell *158*, 633–646. https://doi.org/10.1016/j.cell.2014.05.046.
19. Ivessa, A.S., Zhou, J.Q., Schulz, V.P., Monson, E.K., and Zakian, V.A. (2002). Saccharomyces Rrm3p, a 5' to 3' DNA helicase that promotes replication fork progression through telomeric and subtelomeric DNA. Genes Dev. *16*, 1383–1396. https://doi.org/10.1101/gad.982902.
20. Ivessa, A.S., Lenzmeier, B.A., Bessler, J.B., Goudsouzian, L.K., Schnakenberg, S.L., and Zakian, V.A. (2003). The Saccharomyces cerevisiae helicase Rrm3p facilitates replication past nonhistone protein-DNA complexes. Mol. Cell. *12*, 1525–1536. https://doi.org/10.1016/s1097-2765(03)00456-8.
21. Ivessa, A.S., Zhou, J.Q., and Zakian, V.A. (2000). The Saccharomyces Pif1p DNA helicase and the highly related Rrm3p have opposite effects on replication fork progression in ribosomal DNA. Cell *100*, 479–489.
22. Schmidt, K.H., Derry, K.L., and Kolodner, R.D. (2002). Saccharomyces cerevisiae RRM3, a 5' to 3' DNA helicase, physically interacts with proliferating cell nuclear antigen. J. Biol. Chem. *277*, 45331–45337. https://doi.org/10.1074/jbc.M207263200.
23. Calzada, A., Hodgson, B., Kanemaki, M., Bueno, A., and Labib, K. (2005). Molecular anatomy and regulation of a stable replisome at a paused eukaryotic DNA replication fork. Genes Dev. *19*, 1905–1919. https://doi.org/10.1101/gad.337205.
24. Deegan, T.D., Baxter, J., Ortiz Bazán, M.Á., Yeeles, J.T.P., and Labib, K.P.M. (2019). Pif1-Family Helicases Support Fork Convergence during DNA Replication Termination in Eukaryotes. Mol. Cell. *74*, 231–244.e9. https://doi.org/10.1016/j.molcel.2019.01.040.
25. Rossi, S.E., Foiani, M., and Giannattasio, M. (2018). Dna2 processes behind the fork long ssDNA flaps generated by Pif1 and replication-dependent strand displacement. Nat. Commun. *9*, 4830. https://doi.org/10.1038/s41467-018-07378-5.
26. Prado, F., and Aguilera, A. (2005). Impairment of replication fork progression mediates RNA polII transcription-associated recombination. EMBO J. *24*, 1267–1276. https://doi.org/10.1038/sj.emboj.7600602.
27. Osmundson, J.S., Kumar, J., Yeung, R., and Smith, D.J. (2017). Pif1-family helicases cooperatively suppress widespread replication-fork arrest at tRNA genes. Nat. Struct. Mol. Biol. *24*, 162–170. https://doi.org/10.1038/nsmb.3342.
28. Tran, P.L.T., Pohl, T.J., Chen, C.F., Chan, A., Pott, S., and Zakian, V.A. (2017). PIF1 family DNA helicases suppress R-loop mediated genome instability at tRNA genes. Nat. Commun. *8*, 15025. https://doi.org/10.1038/ncomms15025.
29. Vasiljeva, L., Kim, M., Mutschler, H., Buratowski, S., and Meinhart, A. (2008). The Nrd1-Nab3-Sen1 termination complex interacts with the Ser5-phosphorylated RNA polymerase II C-terminal domain. Nat. Struct. Mol. Biol. *15*, 795–804. https://doi.org/10.1038/nsmb.1468.
30. Zardoni, L., Nardini, E., Brambati, A., Lucca, C., Choudhary, R., Loperfido, F., Sabbioneda, S., and Liberi, G. (2021). Elongating RNA polymerase II and RNA:DNA hybrids hinder fork progression and gene expression at sites of head-on replication-transcription collisions. Nucleic Acids Res. *49*, 12769–12784. https://doi.org/10.1093/nar/gkab1146.

31. Aiello, U., Challal, D., Wentzinger, G., Lengronne, A., Appanah, R., Pasero, P., Palancade, B., and Libri, D. (2022). Sen1 is a key regulator of transcription-driven conflicts. Mol. Cell. *82*, 2952–2966.e6. https://doi.org/10.1016/j.molcel.2022.06.021.

32. Steinmetz, E.J., Warren, C.L., Kuehner, J.N., Panbehi, B., Ansari, A.Z., and Brow, D.A. (2006). Genome-wide distribution of yeast RNA polymerase II and its control by Sen1 helicase. Mol. Cell. *24*, 735–746. https://doi.org/10.1016/j.molcel.2006.10.023.

33. Xie, J., Aiello, U., Clement, Y., Haidara, N., Girbig, M., Schmitzova, J., Pena, V., Müller, C.W., Libri, D., and Porrua, O. (2022). An integrated model for termination of RNA polymerase III transcription. Sci. Adv. *8*, eabm9875. https://doi.org/10.1126/sciadv.abm9875.

34. Alzu, A., Bermejo, R., Begnis, M., Lucca, C., Piccini, D., Carotenuto, W., Saponaro, M., Brambati, A., Cocito, A., Foiani, M., and Liberi, G. (2012). Senataxin associates with replication forks to protect fork integrity across RNA-polymerase-II-transcribed genes. Cell *151*, 835–846. https://doi.org/10.1016/j.cell.2012.09.041.

35. Mischo, H.E., Gómez-González, B., Grzechnik, P., Rondón, A.G., Wei, W., Steinmetz, L., Aguilera, A., and Proudfoot, N.J. (2011). Yeast Sen1 helicase protects the genome from transcription-associated instability. Mol. Cell. *41*, 21–32. https://doi.org/10.1016/j.molcel.2010.12.007.

36. Torres, J.Z., Schnakenberg, S.L., and Zakian, V.A. (2004). Saccharomyces cerevisiae Rrm3p DNA helicase promotes genome integrity by preventing replication fork stalling: viability of rrm3 cells requires the intra-S-phase checkpoint and fork restart activities. Mol. Cell Biol. *24*, 3198–3212.

37. Torres, J.Z., Bessler, J.B., and Zakian, V.A. (2004). Local chromatin structure at the ribosomal DNA causes replication fork pausing and genome instability in the absence of the S. cerevisiae DNA helicase Rrm3p. Genes Dev. *18*, 498–503. https://doi.org/10.1101/gad.1154704.

38. Mohanty, B.K., Bairwa, N.K., and Bastia, D. (2006). The Tof1p-Csm3p protein complex counteracts the Rrm3p helicase to control replication termination of Saccharomyces cerevisiae. Proc. Natl. Acad. Sci. USA *103*, 897–902. https://doi.org/10.1073/pnas.0506540103.

39. Azvolinsky, A., Giresi, P.G., Lieb, J.D., and Zakian, V.A. (2009). Highly transcribed RNA polymerase II genes are impediments to replication fork progression in Saccharomyces cerevisiae. Mol. Cell. *34*, 722–734. https://doi.org/10.1016/j.molcel.2009.05.022.

40. Hazelbaker, D.Z., Marquardt, S., Wlotzka, W., and Buratowski, S. (2013). Kinetic competition between RNA Polymerase II and Sen1-dependent transcription termination. Mol. Cell. *49*, 55–66. https://doi.org/10.1016/j.molcel.2012.10.014.

41. Friedman, K.L., and Brewer, B.J. (1995). Analysis of replication intermediates by two-dimensional agarose gel electrophoresis. Methods Enzymol. *262*, 613–627. https://doi.org/10.1016/0076-6879(95)62048-6.

42. Casper, A.M., Nghiem, P., Arlt, M.F., and Glover, T.W. (2002). ATR regulates fragile site stability. Cell *111*, 779–789.

43. Hashash, N., Johnson, A.L., and Cha, R.S. (2011). Regulation of fragile sites expression in budding yeast by MEC1, RRM3 and hydroxyurea. J. Cell Sci. *124*, 181–185. https://doi.org/10.1242/jcs.077313.

44. Cha, R.S., and Kleckner, N. (2002). ATR homolog Mec1 promotes fork progression, thus averting breaks in replication slow zones. Science *297*, 602–606. https://doi.org/10.1126/science.1071398.

45. Broccoli, S., Rallu, F., Sanscartier, P., Cerritelli, S.M., Crouch, R.J., and Drolet, M. (2004). Effects of RNA polymerase modifications on transcription-induced negative supercoiling and associated R-loop formation. Mol. Microbiol. *52*, 1769–1779. https://doi.org/10.1111/j.1365-2958.2004.04092.x.

46. Sogo, J.M., Ness, P.J., Widmer, R.M., Parish, R.W., and Koller, T. (1984). Psoralen-crosslinking of DNA as a probe for the structure of active nucleolar chromatin. J. Mol. Biol. *178*, 897–919. https://doi.org/10.1016/0022-2836(84)90318-8.

47. Sogo, J.M., Lopes, M., and Foiani, M. (2002). Fork reversal and ssDNA accumulation at stalled replication forks owing to checkpoint defects. Science *297*, 599–602. https://doi.org/10.1126/science.1074023.

48. Gasser, R., Koller, T., and Sogo, J.M. (1996). The stability of nucleosomes at the replication fork. J. Mol. Biol. *258*, 224–239. https://doi.org/10.1006/jmbi.1996.0245.

49. Han, Z., Libri, D., and Porrua, O. (2017). Biochemical characterization of the helicase Sen1 provides new insights into the mechanisms of non-coding transcription termination. Nucleic Acids Res. *45*, 1355–1370. https://doi.org/10.1093/nar/gkw1230.

50. Rivosecchi, J., Larochelle, M., Teste, C., Grenier, F., Malapert, A., Ricci, E.P., Bernard, P., Bachand, F., and Vanoosthuyse, V. (2019). Senataxin homologue Sen1 is required for efficient termination of RNA polymerase III transcription. EMBO J. *38*, e101955. https://doi.org/10.15252/embj.2019101955.

51. Porrua, O., and Libri, D. (2015). Transcription termination and the control of the transcriptome: why, where and how to stop. Nat. Rev. Mol. Cell Biol. *16*, 190–202. https://doi.org/10.1038/nrm3943.

52. Margalef, P., Kotsantis, P., Borel, V., Bellelli, R., Panier, S., and Boulton, S.J. (2018). Stabilization of Reversed Replication Forks by Telomerase Drives Telomere Catastrophe. Cell *172*, 439–453.e14. https://doi.org/10.1016/j.cell.2017.11.047.

53. Azvolinsky, A., Dunaway, S., Torres, J.Z., Bessler, J.B., and Zakian, V.A. (2006). The S. cerevisiae Rrm3p DNA helicase moves with the replication fork and affects replication of all yeast chromosomes. Genes Dev. *20*, 3104–3116. https://doi.org/10.1101/gad.1478906.

54. Bermejo, R., Capra, T., Gonzalez-Huici, V., Fachinetti, D., Cocito, A., Natoli, G., Katou, Y., Mori, H., Kurokawa, K., Shirahige, K., and Foiani, M. (2009). Genome-organizing factors Top2 and Hmo1 prevent chromosome fragility at sites of S phase transcription. Cell *138*, 870–884. https://doi.org/10.1016/j.cell.2009.06.022.

55. Pommier, Y., Leo, E., Zhang, H., and Marchand, C. (2010). DNA topoisomerases and their poisoning by anticancer and antibacterial drugs. Chem. Biol. *17*, 421–433. https://doi.org/10.1016/j.chembiol.2010.04.012.

56. Kim, S., Beltran, B., Irnov, I., and Jacobs-Wagner, C. (2019). Long-Distance Cooperative and Antagonistic RNA Polymerase Dynamics via DNA Supercoiling. Cell *179*, 106–119.e16. https://doi.org/10.1016/j.cell.2019.08.033.

57. Postow, L., Crisona, N.J., Peter, B.J., Hardy, C.D., and Cozzarelli, N.R. (2001). Topological challenges to DNA replication: conformations at the fork. Proc. Natl. Acad. Sci. USA *98*, 8219–8226. https://doi.org/10.1073/pnas.111006998.

58. Postow, L., Ullsperger, C., Keller, R.W., Bustamante, C., Vologodskii, A.V., and Cozzarelli, N.R. (2001). Positive torsional strain causes the formation of a four-way junction at replication forks. J. Biol. Chem. *276*, 2790–2796. https://doi.org/10.1074/jbc.M006736200.

59. Olavarrieta, L., Martínez-Robles, M.L., Sogo, J.M., Stasiak, A., Hernández, P., Krimer, D.B., and Schvartzman, J.B. (2002). Supercoiling, knotting and replication fork reversal in partially replicated plasmids. Nucleic Acids Res. *30*, 656–666.

60. Nowotny, J., Wells, A., Oluwadare, O., Xu, L., Cao, R., Trieu, T., He, C., and Cheng, J. (2016). GMOL: An Interactive Tool for 3D Genome Structure Visualization. Sci. Rep. *6*, 20802. https://doi.org/10.1038/srep20802.

61. Langmead, B., and Salzberg, S.L. (2012). Fast gapped-read alignment with Bowtie 2. Nat. Methods *9*, 357–359. https://doi.org/10.1038/nmeth.1923.

62. Li, D., Purushotham, D., Harrison, J.K., Hsu, S., Zhuo, X., Fan, C., Liu, S., Xu, V., Chen, S., Xu, J., et al. (2022). WashU Epigenome Browser update 2022. Nucleic Acids Res. *50*, W774-w781. https://doi.org/10.1093/nar/gkac238.

63. Karolchik, D., Baertsch, R., Diekhans, M., Furey, T.S., Hinrichs, A., Lu, Y.T., Roskin, K.M., Schwartz, M., Sugnet, C.W., Thomas, D.J., et al.

(2003). The UCSC Genome Browser Database. Nucleic Acids Res. *31*, 51–54. https://doi.org/10.1093/nar/gkg129.

64. Quinlan, A.R., and Hall, I.M. (2010). BEDTools: a flexible suite of utilities for comparing genomic features. Bioinformatics *26*, 841–842. https://doi.org/10.1093/bioinformatics/btq033.
65. Li, H., and Durbin, R. (2009). Fast and accurate short read alignment with Burrows-Wheeler transform. Bioinformatics *25*, 1754–1760. https://doi.org/10.1093/bioinformatics/btp324.
66. Li, H., Handsaker, B., Wysoker, A., Fennell, T., Ruan, J., Homer, N., Marth, G., Abecasis, G., and Durbin, R.; 1000 Genome Project Data Processing Subgroup (2009). The Sequence Alignment/Map format and SAMtools. Bioinformatics *25*, 2078–2079. https://doi.org/10.1093/bioinformatics/btp352.
67. Schneider, C.A., Rasband, W.S., and Eliceiri, K.W. (2012). NIH Image to ImageJ: 25 years of image analysis. Nat. Methods *9*, 671–675. https://doi.org/10.1038/nmeth.2089.
68. Naughton, C., Avlonitis, N., Corless, S., Prendergast, J.G., Mati, I.K., Eijk, P.P., Cockroft, S.L., Bradley, M., Ylstra, B., and Gilbert, N. (2013). Transcription forms and remodels supercoiling domains unfolding large-scale chromatin structures. Nat. Struct. Mol. Biol. *20*, 387–395. https://doi.org/10.1038/nsmb.2509.
69. Saffran, W.A., Welsh, J.T., Knobler, R.M., Gasparro, F.P., Cantor, C.R., and Edelson, R.L. (1988). Preparation and characterization of biotinylated psoralen. Nucleic Acids Res. *16*, 7221–7231. https://doi.org/10.1093/nar/16.15.7221.
70. Chan, Y.A., Aristizabal, M.J., Lu, P.Y.T., Luo, Z., Hamza, A., Kobor, M.S., Stirling, P.C., and Hieter, P. (2014). Genome-wide profiling of yeast DNA:RNA hybrid prone sites with DRIP-chip. PLoS Genet. *10*, e1004288. https://doi.org/10.1371/journal.pgen.1004288.
71. Boguslawski, S.J., Smith, D.E., Michalak, M.A., Mickelson, K.E., Yehle, C.O., Patterson, W.L., and Carrico, R.J. (1986). Characterization of monoclonal antibody to DNA.RNA and its application to immunodetection of hybrids. J. Immunol. Methods *89*, 123–130. https://doi.org/10.1016/0022-1759(86)90040-2.
72. Lopes, M. (2009). Electron Microscopy Methods for Studying In Vivo DNA Replication Intermediates. In DNA Replication: Methods and Protocols, S. Vengrova and J.Z. Dalgaard, eds. (Humana Press), pp. 605–631. https://doi.org/10.1007/978-1-60327-815-7_34.
73. Zellweger, R., and Lopes, M. (2018). Dynamic Architecture of Eukaryotic DNA Replication Forks In Vivo, Visualized by Electron Microscopy. In Genome Instability: Methods and Protocols, M. Muzi-Falconi and G.W. Brown, eds. (Springer New York), pp. 261–294. https://doi.org/10.1007/978-1-4939-7306-4_19.
74. Neelsen, K.J., Chaudhuri, A.R., Follonier, C., Herrador, R., and Lopes, M. (2014). Visualization and interpretation of eukaryotic DNA replication intermediates in vivo by electron microscopy. Methods Mol. Biol. *1094*, 177–208. https://doi.org/10.1007/978-1-62703-706-8_15.
75. Rossi, S.E., Ajazi, A., Carotenuto, W., Foiani, M., and Giannattasio, M. (2015). Rad53-Mediated Regulation of Rrm3 and Pif1 DNA Helicases Contributes to Prevention of Aberrant Fork Transitions under Replication Stress. Cell Rep. *13*, 80–92. https://doi.org/10.1016/j.celrep.2015.08.073.
76. Xie, C., and Tammi, M.T. (2009). CNV-seq, a new method to detect copy number variation using high-throughput sequencing. BMC Bioinf. *10*, 80. https://doi.org/10.1186/1471-2105-10-80.

STAR★METHODS

KEY RESOURCES TABLE

REAGENT or RESOURCE	SOURCE	IDENTIFIER
Antibodies		
Monoclonal ANTI-FLAG. M2	Invitrogen	Cat# F1804, RRID:AB_262044
Anti-DNA:RNA hybrid (S9.6)	Boguslawski, S J et al.(1986)	N/A
Anti-HA (6E2)	Cell Signaling Technology	Cat# 2999, RRID:AB_1264166
Anti-Rpb1 (8WG16)	Santa Cruz Biotechnology	sc-56767
Anti V5-TAG (PK-TAG)	BIO-RAD	Cat# MCA1360G, RRID:AB_1172162
Anti-histone H3	Abcam	Cat# ab1791, RRID:AB_302613
Anti-BrdU (2B1)	MBL	MI-11-3
Anti-Tubulin-alpha	AbD serotec	Cat# MCA78G, RRID:AB_325005
FITC-Donkey Anti-Rat IgG	JIR	Cat# 712-095-153, RRID:AB_2340652
Chemicals, peptides, and recombinant proteins		
Zymo Research DNA Clean Concentrator kit	Zymo research	Cat# D4004
milliTUBE 1mL AFA Fiber	Covaris	Cat# 520130
microTUBE AFA Fiber Pre-Slit Snap-Cap 130 μL	Covaris	Cat# 520045
Dynabeads™ MyOne™ Streptavidin C1	Invitrogen	Cat# 65002
Dynabeads™ Protein G	Invitrogen	Cat# 10004D
Dynabeads™ Protein A	Invitrogen	Cat# 10002D
dATP solution (100 mM)	NEB	Cat# N0440S
T4 DNA ligase	NEB	Cat# M0202M
T4 DNA Polymerase	Promega	Cat# M4215
10mM dNTPs	Life Technologies	Cat# 18427-088
RNase A	Sigma Aldrich	Cat# R6513
Shortcut RNase III	NEB	Cat# M0245S
Proteinase K	Roche	Cat# 3115852001
Hydroxyurea	Sigma Aldrich	Cat# H8627
Propidium iodide	Sigma Aldrich	Cat# 81845
Trioxsalen	Sigma Aldrich	Cat# T6137
bTMP	N/A	N/A
Complete Protease Inhibitor-EDTA free	Sigma Aldrich	Cat# A32965
Alpha-factor Mating Pheromone	GenScript	Cat# 59401-28-4
QBT	QIAGEN	Cat# 19054
QC	QIAGEN	Cat# 19055
QF	QIAGEN	Cat# 19056
QIAGEN Genomic-Tips 100/G	QIAGEN	Cat# 10243
QIAGEN Genomic-Tips 20/G	QIAGEN	Cat# 10223
QIAquick PCR purification Kit	QIAGEN	Cat# 28104
Benzoylated Naphthoylated DEAE-Cellulose	Sigma-Aldrich	Cat# B6385
Pulse Field Certified Agarose (PFCA)	Bio-rad	Cat# 162-0137
Amicon Ultra-0.5 mL 100K	Millipore	Cat# UFC500396
Glycine	Sigma-Aldrich	Cat# G8898
37% formaldehyde solution	Sigma-Aldrich	Cat# 47608
Nocodazole	Sigma-Aldrich	Cat# M1404
Zymolyase (R) 100T	Amsbio	Cat# 120493-1

(*Continued on next page*)

Continued

REAGENT or RESOURCE	SOURCE	IDENTIFIER
Critical commercial assays		
Qubit™ 1X dsDNA HS Assay Kit	Invitrogen	Cat# Q33230
Affymetrix GeneChip S. cerevisiae Tiling 1.0R Array (Sc03b_MR)	Thermo Fisher	Cat# 900645
Illumina Nextseq 550 System Next Generation Sequencer	Illumina	N/A
NextSeq 500/550 High Output Kit v2.5 (150 Cycles)	Thermo Fisher	Cat# 20024907
GenomePlex complete WGA kit	Sigma Aldrich	Cat# WGA2-50Rx
SeqPlex DNA Amplification Kit	Sigma Aldrich	Cat# SEQXE-50Rx
Deposited data		
NGS and Microarray data	This paper	GEO: GSE214930
Raw images and blots	This paper	https://doi.org/10.17632/v67xz7swfs.1
Code availability	This paper	https://doi.org/10.5281/zenodo.7974524
Experimental models: Organisms/strains		
Please refer to Table S4 as extended data Table related to STAR* METHODS	This paper	N/A
Oligonucleotides		
ARS305F: CTCCGTTTTTAGCCCCCCGTG	This paper	N/A
ARS305R: GATTGAGGCCACAGCAAGACCG	This paper	N/A
TER302F: GAAGGTTCAACATCAATTGATTGAT TCTGCCGCCATGATC	This paper	N/A
TER302R: GCTTCCCTAGAACCTTCTTATGT TTTACATGCGCTGGGTA	This paper	N/A
Software and algorithms		
rMAT	Nowotny, et al.[60]	http://www.bioconductor.org/packages//2.11/bioc/html/rMAT.html
FASTX	N/A	http://hannonlab.cshl.edu/fastx_toolkit/
PICARD	N/A	https://broadinstitute.github.io/picard/
Bowtie2	Langmead, et al.[61]	http://bowtie-bio.sourceforge.net/bowtie2/index.shtml
MACS2	N/A	https://pypi.org/project/MACS2/
WashU Browser	Li, et al.[62]	https://epigenomegateway.wustl.edu/
UCSC browser	Karolchik, et al.[63]	https://genome.ucsc.edu/
BEDtools	Quinlan, et al.[64]	https://bedtools.readthedocs.io/en/latest/
Cutadapt	https://doi.org/10.14806/ej.17.1.200	https://cutadapt.readthedocs.io/en/stable/
BWA	Li, et al.[65]	http://bio-bwa.sourceforge.net/
SAMtools	Li, et al.[66]	http://www.htslib.org/
Flow-Jo	N/A	https://www.flowjo.com/
ImageJ Fiji	Schneider, et al.[67]	https://imagej.nih.gov/ij/download.html

RESOURCE AVAILABILITY

Lead contact

Further information and request for resources and reagents including protocols and synthesized molecules, should be directed to and addressed by lead contact, Marco Foiani (marco.foiani@ifom.eu).

Materials availability

Reagents, protocols and yeast strains from this study, are available upon request with a completed Materials Transfer Agreement.

Data and code availability

- The NGS and Microarray data from this publication have been deposited and are publicly available as of the date of publication. Accession numbers are listed in the key resources table as GEO: GSE214930.
- Original codes used for this publication to analyze data are available at GitHub repository with DOI https://doi.org/10.5281/zenodo.7974524.
- Any additional information required to reanalyze the data reported in this paper is available from the lead contact upon request.

EXPERIMENTAL MODEL AND STUDY PARTICIPANT DETAILS

Yeast growth conditions and cell cycle synchronizations

All yeast strains are W303 derivatives (see Table S4, related to STAR* METHODS). Strains were grown at 25-28°C in YPG (2% Galactose) and moved to YPD (2% Glucose) to induce degradation of the *sen1*^{degron} gene product. For synchronization experiments, cells were pre-arrested in G1 by using α factor 3–5 μg/ml for 2-3hrs, washed twice in YPD medium and released into cell cycle as indicated in figure legends. 0.2M HU or 10 μg/ml of Nocodazole in 1/% DMSO were added to arrest cells in S or G2/M, respectively. When indicated, the arrest nocodazole arrest was maintained by re-adding 10 μg/mL of Nocodazole. For spot assay-based viability score, cells grown in stationary phase were counted and 10-fold serial dilutions were performed in YPD (Glucose 2%), YPG (Galactose 2%) or YPR (Raffinose 2%) plates. The plates were then incubated for 2–4 days at the indicated temperatures and scanned.

METHOD DETAILS

FACs (fluorescence activated cell sorter) analysis

1x10^7 cells were fixed with 70% ethanol. Cells were then treated with 2 mg/mL (final concentration) RNAseA (Sigma) in Tris-HCl 50mM pH7.5 for at least 1 h at 37°C. Later, cells were stained with 50 μg/ml Propidium Iodide (PI) (Sigma) in Buffer solution (180mM Tris-HCl pH7.5, 190mM NaCl, 70mM $MgCl_2$). PI-stained cells were diluted 1:10 in 50mM Tris-HCl pH7.5 and sonicated for 6–8 s at 15–20% sonication power and analyzed with Becton Dickinson FACScan for FL2H fluorescence. Data were analyzed and plotted using Flow-Jo.

Immunofluorescence-IF staining

1-2x10^7 cells were centrifuged and washed with 1x PBS. Cells were crosslinked using 1% formaldehyde solution at RT for 15 min and then quenched using glycine for 5 min. Cells were treated with Zymolase (1 mg/ml) in osmotic solution to prepare spheroplast for 5–15 min at RT. Cells were then washed twice with PBS 1X (137mM NaCl, 10mM Na_2HPO_4, 1.76mM KH_2PO_4, 2.7mM KCl, pH7.4) and stored at 4°C. Cells were then pelleted, applied on glass slides and fixed with acetone and ethanol combination and later incubated with Rat Anti-Tubulin-alpha antibody followed by incubation with secondary antibody FITC-Donkey-Anti-Rat IgG. Immediately before IF imaging by delta vision microscopy, DAPI (0.5 μg/ml) containing vectashield antifade mounting medium was added for 20 min; analysis was carried out using Hoest/DAPI and FITC filters.

bTMP-seq

To map genome wide negative supercoiling, we used the previously described method[10,68] and modified it for sequencing. Biotinylated-TMP synthesis performed as previously described method.[69] 1-8 x10^9 cells were treated with Sodium Azide (0.1%) and kept on ice for 20 min. Cells were collected by centrifugation and the pellets were treated with 800μL of Polyethylene glycol (PEG 50%), 100μL of lithium acetate (1M) and 100μL of DMSO-Dimethyl sulfoxide. Permeabilized yeast cells were incubated with bTMP (calculate as 400μg per 2x10^9 cells) in dark for 90 min and then cross-linked by 365nm UV light at 2000 energy (Millijoules/cm^2) 4 times to form psoralen adducts between two DNA strands. Cells were washed twice with ice-cold 1xPBS and lysed with 1mL lysis buffer (50mM HEPES-KOH pH7.5, 140mM NaCl, 1mM EDTA, 1%Triton X-100, 0.1% Na-deoxycholate) using Zirconia beads. Cells were lysed with PowerLyzer 24 Homogenizer at 4000rpm for 20sec 8 times. In between each round the cells were kept on ice for 5 min. Further, the crosslinked chromatin was sheared to an average size of 100-150bp by covaris focused ultrasonicator E220 and the sonicated samples were incubated with 30μL of 20% SDS, Proteinase K 25μL, RNAseA 5μL and then incubated overnight at 50°C. DNA was purified using QIAquick PCR purification kit. The concentration of the DNA was measured using nano drop. Input DNA was collected from the purified sheared chromatin (1/100 of the material was collected as Input) and stored at −20°C. The purified DNA was incubated with Dynabeads MyOne streptavidin overnight at 4°C. The beads were washed twice with each of the following buffers; wash buffer-I (20mM Tris-HCl pH8, 2mM EDTA, 150mM NaCl, 1%Triton X-, 0.1% SDS), wash buffer-II (20mM Tris-HCl pH 8, 2mM EDTA, 500mM NaCl, 1% Triton X-, 0.1% SDS), wash buffer III (250mM LiCl, 10mM Tris pH8.0, 0.5%Na-deoxycholate, 0.5% NP-40, 1mM EDTA) and 1xTE (20mM Tris pH 8.0, 2mM EDTA). The bTMP–DNA complexes were eluted from the beads using 250μL elution buffer (95% formamide, 10mM EDTA) at 90°C for 20 min and the eluted samples were cleaned with concentration kit from Zymoresearch. From this step onwards, Input and IP DNA were subjected to Whole Genome Amplification using SeqPlex DNA amplification kit (Sigma-Aldrich) and processed for next generation sequencing.

Protein-ChIP-seq

ChIP-seq analysis for proteins was carried out as described[10,54] with few modifications. Cells were cross-linked with 1% formaldehyde in culture medium for 30 min at room temperature followed by quenching with 0.125 M glycine for 5 min and transferred to ice for 20 min. Cells were washed twice with ice-cold 1xPBS and lysed in 1mL of lysis buffer (50mM HEPES-KOH pH7.5, 140mM NaCl, 1mM EDTA, 1%Triton X-100, 0.1%Na-deoxycholate) using Zirconia beads. Cells were lysed with PowerLyzer 24 Homogenizer at 4000 rpm for 20 s for 8 rounds. In between each round the cells were kept on ice for 5 min. The samples were collected from glass beads and centrifuged to collect the pellet at 13400 RCF for 10 min at 4°C. The samples are sonicated to an average size of 100-150bp using covaris focused ultrasonicator E220 with milliTUBE 1mL AFA Fiber (Parameters: Duty Factor 6, burst/cycle 200, Peak Watt 200, Time 2400 s). The samples were centrifuged at 16000 RCF for 5 mins at 4°C and supernatant was collected. The lysate was then centrifuged to remove cell debris and the chromatin fractions were incubated with respective Dynabeads protein beads coated with respective antibody overnight at 4°C. The immune complexes were washed with the following buffers 2 times with ChIP-lysis buffer (50mM HEPES-KOH pH7.5, 140mM NaCl, 1mM EDTA, 1% Triton X-100, 0.1% Na-deoxycholate), 2 times with lysis buffer + high salt (ChIP lysis buffer +360 mM NaCl), 2 times with ChIP-wash buffer (250mM LiCl, 10mM Tris pH8.0, 0.5%Na-deoxycholate, 0.5%NP-40, 1mM EDTA) and 2 times with 1xTE (20mM Tris pH8.0, 2mM EDTA). The protein-DNA complexes were eluted from the beads using 250 μL elution buffer (1%SDS, 50mM Tris pH8.0, 10mM EDTA) at 65°C for 20 min followed by the addition of proteinase K at 500 μg/mL and overnight incubation at 65°C. Input DNA was isolated from sheared chromatin input (1/100 of the material used for ChIP). The IP and Input samples were purified with DNA clean and concentration kit from Zymoresearch and eluted in elution buffer from the kit. The input samples were analyzed in Agilent bioanalyzer for optimum fragmentation. Both Input and IP samples were processed for sequencing and ChIP–seq libraries were prepared according to the manufacturer's protocols. The Input and IP samples were ligated with illumina barcodes and amplified using Kapa library amplification kit, followed by size selection with AMPure XP Beads. ASPRI clean-up with a 1.5xAMPure XP Bead: DNA ratio was performed and final libraries were eluted and sequenced using Illumina Nextseq 550 System with NextSeq 500/550 High or medium Output Kit v2.5 where each sample (IP and Input) contained approximately 10 million paired end reads.

DRIP-chip

DRIP-ChIP was performed using anti-RNA:DNA hybrid monoclonal mouse antibody S9.6 as previously described.[10,70] The method was adopted with a few changes; cells were cross-linked by shaking with 1% formaldehyde in culture medium for 20 min at room temperature and the reaction was quenched with 0.125 M glycine for 5 min at RT. Cells were centrifuged and washed twice with ice-cold 1xPBS and lysed in 1 mL of lysis buffer (50mM HEPES-KOH pH7.5, 140mM NaCl, 1mM EDTA, 1%Triton X-100, 0.1% Na-deoxycholate) using Zirconia beads. Cross-linked chromatin was sheared to an average size of 300–500 bp by 6x15-s pulses using a Biorupter sonicator. The lysate was then centrifuged to remove cell debris and collected as chromatin fraction at 4°C. The chromatin fraction was incubated with Protein-A magnetic beads coated with anti-DNA:RNA hybrid-S9.6 antibody[71] overnight at 4°C. The immune complexes were washed twice with the following buffers- ChIP-lysis buffer (50mM HEPES-KOH pH7.5, 140mM NaCl, 1mM EDTA, 1% Triton X-100, 0.1% Na-deoxycholate), lysis buffer+ high salt (ChIP lysis buffer +360mM NaCl), ChIP-wash buffer (250mM LiCl, 10mM Tris pH8.0, 0.5% Na-deoxycholate, 0.5%NP-40, 1mM EDTA) and 1xTE (20mM Tris pH8.0, 2mM EDTA). The RNA:DNA hybrid complexes were eluted from the beads in 250μL elution buffer (1%SDS, 50mM Tris pH8.0, 10mM EDTA) at 65°C for 20 min followed by the addition of proteinase K at 500 μg/ml and incubated overnight at 65°C. Input DNA was isolated from sheared chromatin input (1/100 of the material used for ChIP). Both IP and input samples were processed as mentioned in the section below 'Microarray and data processing'.

ChIP-seq data analysis

The raw reads were aligned to the reference genome (SacCer 2011) using bowtie2 to produce an alignment file (BAM). The aligned reads were sorted by genomic coordinates and indexed using samtools. The PCR duplicates were removed from the sorted BAM file using PICARD tools. The BAM files were sorted and indexed for the peak calling using samtools. The bedgraph files were generated using bamCompare from deepTools by comparing BAM files of IP and Input (IP read coverage/Input read coverage) resulting in a ratio for every base across the whole genome. For Protein ChIP-seq, MACS2 peak calling tool was used to produce bed files containing peaks/enriched regions using the following parameters (–gsize = 1.21e+7, -q 0.05). The bed and bedgraph files were visualized using UCSC genome browser and WashU Epigenome browser.

Microarray processing

In case of ChIP-chip, BrdU-chip and DRIP-chip, samples were measured using nanodrop and 5000ng of Input and IP was used for the further steps. Both IP and input DNA were amplified using the GenomePlex complete whole-genome amplification kit, they were then biotin-labelled and hybridized to Affymetrix GeneChip *S. cerevisiae* Tiling 1.0R Array (Sc03b_MR) according to the Affymetrix standard protocol. Biotin labelling was performed using 4.85μL of 10XOne-Phor-All Buffer, 25mM CoCl2, 2.9μL DNAase reaction mix 1.5μL and 5μg of DNA (IP or Input) with ddH2O in 40.75μL. Samples were vortexed, pulse-spun and incubated in thermocycler at 37°C for 30 s and then transferred to 95°C for 15 min. Samples were transferred to new 1.5mL Eppendorf tube and DNA labelling was performed using 5μL of TdT reaction buffer, 1μL Biotin-N11-ddATP (1nMole/μl) and 1μL terminal transferase (400U/μl). Samples were incubated at 37°C for 1hr.

In-vivo psoralen crosslinking of the DNA for EM analysis

Psoralen efficiently intercalates in the double strand DNA and upon irradiation with ultraviolet (UV) light (365 nm) forms covalent crosslinks between pyrimidines of opposite strands. Psoralen derivatives easily penetrate the membranes of living cells and Trimethylpsoralen (TMP) is the most commonly Psoralen solution: 0.2 mg/ml Trioxalen (SIGMA) in 100% Ethanol. Always keep covered with aluminum in the dark at −20°C. 1-2x10^9 cells (200mL from a 1x10^7 cells/ml culture) were collected. Cells were blocked by treating with sodium azide (0.1%) for 5 min or more in ice. Cells were pelleted and washed with 20mL of ice-cold water. It was then re-suspended in 5mL ice-cold water and transferred to a 6 well plate (1sample/well). The 6 well plates were always kept in ice while performing psoralen-crosslinking. 300μL of psoralen solution was added, mix well and incubated for 5 min (in ice). after 5 min, it was mixed again and irradiated for 10 min (in ice) in a Stratalinker (Stratagene) with 365 nm UV bulbs, at a distance of 2–3 cm from the bulbs. These steps were repeated three more times. The cells were transferred to falcon tubes and the plate was washed with 5 mL of ice-cold water to collect all cells. The cells were pelleted for DNA extraction.

Genomic DNA extraction (for EM, BrdU-chip and CNVs)

Genomic DNA isolation was performed as per manufactures instructions (QIAGEN Genomic DNA). In brief, 200 mL of a culture of 1X10^7cells/ml were harvested. Cells were blocked with 0.1% of Sodium Azide (final concentration), kept at least 5 min in ice, centrifuged at 6000–8000 rpm for 5 min and washed with 20mL of ice-cold water. The cells were transferred to a 50mL Falcon tube, re-suspended in 5mL of Y1 yeast lysis buffer (1M Sorbitol, 100mM EDTA, 14mM β-mercaptoethanol supplemented with 500μL/sample of Zymolyase solution 10 mg/ml) and incubated for 30 min at 30°C (spheroplast). The spheroplasts were collected by centrifugation at 4000rpm for 10 min at 4°C. The supernatant was discarded and the spheroplasts were re-suspended in 4 mL of G2 digestion buffer (800mM guanidine HCl, 30mM Tris-HCl pH8.0, 30mM EDTA pH8.0, 5% Tween 20, 0.5%Triton X-100). 100μL of RNase A was added and incubated for at least 30 min at 37°C. 200μL of Proteinase K was added and incubated for 2 h at 50°C and 100μL of Proteinase K was again added and incubated overnight at 30°C. The lysate was centrifuged for 10 min at 4000 rpm at 4°C. The supernatant was diluted with an equal volume (4mL) of QBT buffer (Equilibration Buffer) 750mM NaCl, 50mM MOPS pH7.0.15% Isopropanol, 0.15%Triton X-100. The diluted supernatant was loaded on the Qiagen tip 100G-anion exchange column, pre-equilibrated with 4 mL of QBT buffer. It was washed twice with 7.5mL of QC wash buffer (1M NaCl, 50mM MOPS pH 7.0, 15% isopropanol) eluted with 5 mL warm QF elution buffer (1.25M NaCl, 50mM Tris-HCl pH8.5, 15%Isopropanol) in a corex glass tube. It was then precipitated with 3.5 mL of isopropanol and centrifuged at 8500 rpm for 10 min in a Beckman JS 13.1 swinging bucket rotor. The pellet was washed with 1 mL of ice-cold 70% Ethanol and re-suspend in 250μL of 10mM Tris-HCl pH 8.0 and stored at 4°C.

BrdU-chip

Yeast culture was grown O/N as log at 23°C in SC-URA medium until up to 1x10^7 cells/ml. The synchronization was done in YPD or YPG medium using α-Factor at 23°C. After synchronization, BrdU 200 μg/ml was added for 20 min before the release. Cells were released from G1 into YPD medium containing BrdU 200 μg/ml. Cell were blocked using 0.1% of Sodium Azide and kept on ice for at least 5 min. Cells were pellet centrifuged and washed with 20mL of cold and sterilized 1xTE. Genomic DNA was isolated as mentioned in the genomic DNA extraction section and the DNA was re-suspended in 250 μL of 1xTE pH8. For each 200mL culture genomic DNA, 20μL Protein A dynabeads (Invitrogen) were washed twice in a costar prelubricated tube with 1mL of 1xPBS, 5 mg/ml BSA, 0.1% Tween 20. The beads were re-suspended in 20μL of 1x PBS, 5 mg/ml BSA, 0.1% Tween 20 and add 4μg of anti-BrdU antibody (MBL M1-11-3). This complex was incubated O/N at 4°C. BrdU containing genomic DNA was fragmented to 200-500bp using the bandelin UW2070 sonicator with following parameters as 20% power, 20 s/pulse for 6 times. Fragmented DNA was quantified and antibody-bead complex was washed two times with 1mL of 1xPBS, 5 mg/ml BSA, 0.1% Tween 20. Beads were resuspended in 20μL and split into 2 costar prelubricated tubes. The DNA was denatured at 100°C for 10 min and immediately put on ice and 100μL of 2xPBS and 200μL of ice-cold 1xPBS, 2% BSA, 0.2%Tween 20 was added. 10μL of antibody-beads complex was added in denatured DNA and incubated O/N at 4°C rotating. Beads containing tubes were kept on magnetic grid and washed as following, 2 times with ChIP lysis buffer (50mM Hepes-KOH pH7.5, 140mM NaCl, 1mM EDTA, 1% Triton X-100, 0.1% Sodium deoxycholate), 2 times with (ChIP Lysis buffer +500mM NaCl), 2 times with ChIP Washing buffer (10mM Tris-HCl pH8.0, 250mM LiCl, 0.5% NP-40, 0.5% Sodium deoxycholate, 1mM EDTA) and one wash with 1xTE pH8.0 and all residual liquid was removed with vacuum pump. The beads were re-suspended in 50μL of ChIP Elution buffer (50mM Tris-HCl pH8.0, 10mM EDTA, 1%SDS) and incubated at 65°C for 10 min. To the eluted material (IP) and Input, 49μL of 1xTE, 1μL of Proteinase K (Stock 50 mg/mL) was added and incubated at 37°C for 1hr and the DNA was purified by Qiagen PCR purification Kit and eluted with EB buffer. IP and Input samples proceeded with WGA (Whole Genome Amplification) using WGA2 GenomePlex Complete Genome Amplification (WGA) Kit as per manufacturer's instructions.

TEM analysis of replication intermediates

After crosslinking and purification of genomic DNA as mentioned above, Transmission Electron Microscopy visualization of replication intermediates was performed as previously reported[72–74] as native and denaturing condition. In brief, 5-10μg of genomic DNA was partially digested with the PvuI and applied to 0.3 g/mL BND cellulose[73] equilibrated with 10mM Tris-HCl, pH8.0, 300mM NaCl

for 10 min at RT. After washing with 10mM Tris-HCl, pH8.0, 1mM NaCl, ssDNA-enriched DNA was eluted with 10mM Tris-HCl, pH8.0, 1mM NaCl, 2% caffeine (freshly prepared). Samples were enriched using 100kD cut off amicon filtration columns and washed-out residual buffer. Fractions of the samples were quantified on nano drop and agarose gel. Later, samples were spread onto a water surface in the presence of BAC (Benzalkonium Chloride) and the DNA molecules in the presence of uranyl acetate were spread in monomolecular layer and adsorbed on carbon-coated EM grids. To analyzed structures and visualize DNA molecules, platinum-based low angle rotatory shadowing used. The thickness of DNA filaments distributed was around 100A^{o} (10 nm). The TEM pictures were acquired using an FEI Tecnai 12 G2 spirit Biotwin microscope operated at 120 kV (KV) in TEM bright-field mode, and a side-mounted optical fibered Gatan Orius SC-1000 camera (11 megapixels) was utilized to generate the TEM images.

The average thickness of the DNA fibers was distributed around 10 nm. The conversion factor for the calculation of the DNA fibers length was 0.36 nm/base pair and was established through the measurement of the length of plasmid DNA molecules of known dimensions utilized as internal standards. The pixel size was calibrated at each magnification using the GATAN digital micrograph software. The pixel size was corrected automatically at each magnification according to the internal calibrations of the electron microscope and camera.

Pulse field gel electrophoresis (PFGE)

Pulse Field Gel Electrophoresis (PFGE) was performed as described previously.[3,75] In brief, cells were harvested at given time point and treated with sodium azide and kept on ice for 20 min and washed with ice-cold 1xPBS. For each time point pellet was re-suspended in PFGE-Solution I (SCE-1M Sorbitol, 0.1M Sodium Citrate, 0.06M EDTA pH8.0), 0.2% β-mercaptoethanol, 1 mg/ml Zymolyase (100U/ml, 50μL for each plug) and add an equal volume of 50°C molten PFCA (1% Pulse Field Certified Agarose (PFCA), and mixed with a pipette. Plug-cast (BIOR-RAD) was filled with cell/agarose mix (approximately 90-100μL per plug) And left for 20 min at RT and 10 min at 4°C. Plugs were ejected in 50mL Falcon tube and covered with Solution I (0.5 mL per plug). It was then left at 37°C for 1 h. Solution I was removed gently and the plugs were washed with an abundant volume of 0.5M EDTA pH8.0. The plugs were re-suspended in Solution II (0.5M EDTA pH8.0, 0.1%Sarkosyl, 1 mg/ml Proteinase K) (0.5mL per plug) and incubated O/N at 37°C. Solution II was discarded and washed 3 times with an abundant volume of 1xTE pH8.0. The plugs were transferred in a new 50 mL falcon tube and washed for 2 h with 1xTE pH 8.0 on a rotating wheel. The plugs to be analyzed were transferred to an Eppendorf tube and equilibrated for 1 h in the running buffer of the gel (0.5xTBE) on a rotating wheel. Electrophoresis was performed on a 1% pulse field agarose gel for 24 h at 200 V with 60 s pulses followed by 90sec pulses in 0.5xTBE at 14°C (CHEF-DR III Pulsed Field Electrophoresis Systems) apparatus. The gel was stained with 0.3μg/ml Ethidium Bromide for 30 min and then subjected to Southern blot. The membrane was then hybridized with a radiolabelled probe against specific region on the chromosome.

Copy number variation sequencing

We adapted a previously described method to score CNVs.[76] Genomic DNA extraction was performed with the Qiagen genomic Kit as mentioned above. Genomic DNA was sonicated to the medium length of 100–150 bp with covaris sonication and Ion Proton sequencing platform was performed. Libraries for sequencing were prepared following the manufacturer protocols (Thermo Fisher Scientific/Life Technologies). Briefly, 1μg of fragmented DNA was end repaired and adapter ligated using the KAPABiosystems Library Prep kit for Ion Torrent (KAPABiosystems, inc) and adapter barcode KAPA for Ion Torrent 1–16. After adapter ligation each sample was size selected using AMPure XP Bead (Beckman Coulter, inc). An amplification reaction was set up for a final volume of 50μL. An SPRI cleanup (Solid Phase Reversible Immobilization method) with a 1.5X Bead:DNA ratio was performed post amplification and final libraries were eluted in 25μL. Libraries were quantified on Qubit fluorometer with HS DNA (Thermo Fisher Scientific/Life Technologies) and checked for size on Agilent Bioanalyzer with HS DNA kit (Agilent, Santa Clara, CA). Each size selected library was diluted according to the final concentration of 11pM and clonally amplified using the Ion Proton Hi-QTemplate Kit (Thermo Fisher Scientific/Life Technologies) with IonOneTouch 2 instrument (Thermo Fisher Scientific/Life Technologies). After emulsion PCR, DNA positive ISPs were recovered and enriched according to standard protocols with the IonOneTouch ES Instrument (Thermo Fisher Scientific/Life Technologies). A sequencing primer was annealed to DNA positive and sequencing polymerase bound ISPs (Ion Sphere Particles). ISPs loaded into Ion P1 sequencing chips. Sequencing of the samples was conducted according to the Ion ProtonHi-Q Sequencing Kit Protocol. One P1 sequencing chips with 10 libraries were loaded and run on an Ion Proton sequencer.

CNV data analysis

The following steps were used to process the Copy number variation data generated from Ion Proton sequencer. Alignment was performed using TMAP Toolkit software, where yeast reference genome 2011 version (sacCer3) was used to align the filtered raw reads to obtain the BAM file. The aligned BAM files were then sorted using the samtools. The sorted bam file was used to generate bedgraph file containing read count for every base across the genome using bedtools genomecov. The 200 bases window and 50 bases sliding window was used to build an interval file across the whole genome. For better result, the median read length as the window size and 1/5th of the median read length as the sliding window size were used for building the interval file. For each calculated window, the number of mapped hits was counted, normalized and ratio was calculated with respect to the reference to obtain CNVs (amplification/deletion). The CNVs for each genotype and conditions, were compared with the functional sites such as replication

termination, telomeres, replication origin, high transcribing ORFs, fragile sites, hybrids and protein binding sites etc. Customized python and R-scripts were used for the graph generation and statistical calculations.

QUANTIFICATION AND STATISTICAL ANALYSIS

The microarray and meta-gene data analysis were performed as previously described.[10,70] The significant enrichment (calculation of p *value*) of RNA-DNA hybrid, CNV, BrdU and protein binding on genomics features such as telomere, termination regions and ORFs were carried out using bedtools fisher exact test.